Corrosion of Carbon Steel Under Disbonded Coatings in Acidified Leaching Processes

A Thesis Submitted to the College of

Graduate Studies and Research

In Partial Fulfillment of the Requirements

For the Degree of Master of Science

In the Department of Chemical and Biological Engineering

University of Saskatchewan

Saskatoon

By

Maryam Tolouei Asbforoushani

PERMISSION TO USE

In presenting this thesis in partial fulfilment of the requirements for a Postgraduate degree from the University of Saskatchewan, I agree that the Libraries of this University may make it freely available for inspection. I further agree that permission for copying of this thesis in any manner, in whole or in part, for scholarly purposes may be granted by the professors who supervised my thesis work or, in their absence, by the Head of the Department or the Dean of the College in which my thesis work was done. It is understood that any copying or publication or use of this thesis or parts thereof for financial gain shall not be allowed without my written permission. It is also understood that due recognition shall be given to me and to the University of Saskatchewan in any scholarly use which may be made of any material in my thesis.

Requests for permission to copy or to make other use of material in this thesis in whole or part should be addressed to:

Head of the Department of Chemical and Biological Engineering

57 Campus Drive

University of Saskatchewan

Saskatoon, Saskatchewan S7N 5A9

Canada

ABSTRACT

In this research, corrosion behaviour of A36 carbon steel under engineered disbonded coating was investigated in sulphuric acid solutions containing sodium chloride and iron (III) sulphate. Scanning electron microscopy (SEM) and x-ray diffraction (XRD) analyses were carried out to study the morphology and phase composition of corrosion products formed on the carbon steel surface. The results of the SEM analysis showed that only general and pitting corrosion occurred on the carbon steel surface with the engineered crevice. The size of the pits increased as the sulphuric acid and sodium chloride concentrations increased. Moreover, the corrosion products had an open, irregular and loose structure at the pits mouth. The loose and open structure of the corrosion products facilitates diffusion of chloride ions, oxygen, water and contaminants into the carbon steel surface. In contrast, the corrosion products had a very compact and continuous structure outside the pits which provided a good protection against further corrosion.

The x-ray diffraction analysis showed that the corrosion products layer mainly consisted of lepidocrocite (γ-FeOOH), goethite (α-FeOOH) and iron sulphide (FeS) on the crevice edges. The Pourbaix diagram of iron in sulphuric acid solution at room temperature indicates that iron sulphide is formed on the metal surface at different pH values. The akaganeite (β-FeOOH) diffraction peak was not identified in any spectrum which could be due to the low concentration of chloride ions in the solutions. Furthermore, the number of lepidocrocite peaks decreased as the sulphuric acid concentration increased from 10 g l^{-1} to 50 g l^{-1}. The lepidocrocite is dissolved in the presence of sulphuric acid, and the dissolved ion acts as an oxidant to the metal and hence lower lepidocrocite peaks are identified.

Electrochemical noise measurement (ECN) testing was also performed to investigate the corrosion process occurring on the carbon steel surface with the engineered crevice. The results of the ECN measurements showed that current increased during first few minutes and then decreased slightly. Also, the coupled potential did not change after an initial shift in negative direction. The low current flowing through the carbon steel electrodes and the constant potential showed that the crevice corrosion did not develop. These results imply that the crevice corrosion may not occur on the carbon steel surface in acidic solutions containing chloride ions.

ACKNOWLEDGEMENTS

I would like to express my deepest gratitude and appreciation to my supervisor, Prof. Richard W. Evitts who was more of a friend and mentor, than a professor. I acknowledge him for the great leadership and support and valuable advice during my graduate studies. Thank you very much for the words of inspiration and encouragement throughout this research. I would especially like to thank my co-supervisor, Dr. Kevin L. Heppner for the brilliant suggestions and comments as well as friendship throughout my master program. I really appreciate his expertise and valuable knowledge on the way of my research.

I would also like to extend my sincere appreciation to my committee members, Prof. Akindele Odeshi, Prof. Venkatesh Meda and Prof. Corey Owen for their great suggestions. Moreover, I acknowledge the financial supports from the Natural Science and Engineering Research Council of Canada (NSERC) and the Department of Chemical and Biological Engineering of the University of Saskatchewan.

At the end, I would like to thank my husband, Davood Ghadiri, for his endless love and amazing support. I believe that this work would not be possible without his support. Thank you so much for accompanying me on this amazing adventure that resulted in the present thesis.

DEDICATION

I dedicate this thesis to my Husband, my parents and my brother.

Thank you very much for your love and encouragement throughout my life.

TABLE OF CONTENTS

LIST OF TABLES

Table **Page**

LIST OF FIGURES

Figure **Page**

NOMENCLATURE

Acronyms

ECN	Electrochemical Noise Measurement
EIS	Electrochemical Impedance Spectroscopy
RE	Reference Electrode
RO	Reverse Osmosis
SCE	Saturated Calomel Electrode
SEM	Scanning Electron Microscopy
WE	Working Electrode
XRD	X-ray Diffraction
EDS	Energy Dispersive X-ray Spectroscopy
ZRA	Zero Resistance Ammeter

Chemicals

Fe^{2+}	Iron (II)
Fe^{3+}	Iron (III)
α-FeOOH	Goethite
β-FeOOH	Akaganeite
γ-FeOOH	Lepidocrocite
Fe_2O_3	Hematite
Fe_3O_4	Magnetite
FeS	Iron (II) Sulphide
$FeSO_4$	Iron (II) Sulphate
$Fe_2(SO_4)_3$	Iron (III) Sulphate

NaCl	Sodium Chloride
$NaClO_3$	Sodium Chlorate
H_2SO_4	Sulphuric Acid

Symbols

I_g	Current Noise (A)
E	Potential (V)
r	Area Ratio of Cathode to Anode
E_p	Pitting Potential (V)
A	Anion Concentration (eq l^{-1})

Chapter One

1 Introduction

1.1 Background

Carbon steel and austenitic stainless steels are the most widely used construction materials to handle sulphuric acid solutions. Carbon steel is an inexpensive alloy; however, its usage requires a comprehensive understanding of its corrosion behaviour in corrosive environments (Panossian *et al*., 2012). Rubber coatings are often used to protect carbon steel equipment against corrosion in hydrometallurgical circuits. A major failure of the rubber coatings is the disbonding of the coating due to chemical and/or mechanical actions (Schweitzer, 2007). The disbondment of the coating will form a gap between the coating and the carbon steel substrate that may significantly increase the tendency of the substrate for degradation via general, pitting and crevice corrosion. Pitting and crevice corrosion are considered important concerns if metals are exposed to chloride containing solutions. Several factors affect the occurrence and rate of crevice and pitting corrosion including alloy composition, geometry, pH, dissolved ions concentrations and temperature (Kawashima *et al*., 1997; Zhao and Zuo, 2007; Wang *et al*., 2014). In this research the geometry of the crevices and crevice thicknesses were chosen based on the crevice corrosion scaling law as shown in Fig. 1.1.

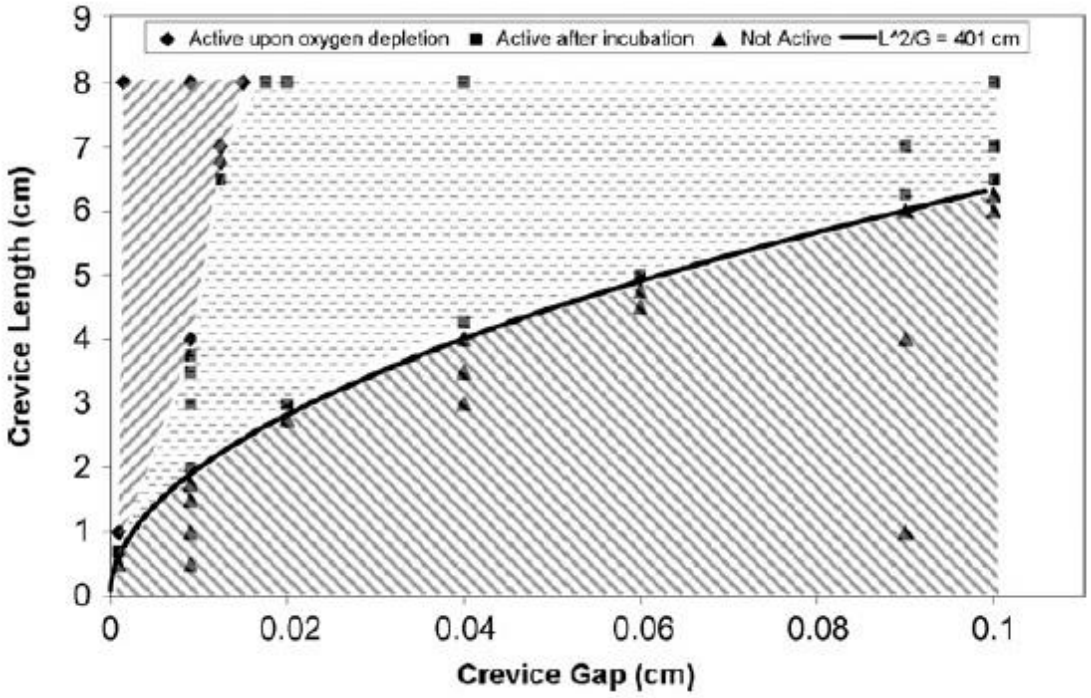

Fig. 1.1 Critical aspect ratio for crevice corrosion (Kennel *et al*., 2009)

The crevice corrosion is difficult to detect since it remains a dangerous phenomenon under the disbonded coating. It is a form of localized attack that happens in areas of the metal or alloy surface in contact with a stagnant solution while the most part of the surface is exposed to the bulk solution. Although the crevice corrosion may occur on the metal surfaces which are not covered by passive films, but it occurs frequently on passivated metal surfaces. However, pitting corrosion occurs only at the passivated metal surfaces (Marcus, 2002).

The passive film is not formed on the carbon steel surface since chromium (Cr) does not exist in its composition. Chromium is responsible for the formation of a thin passive layer of chromium oxide (Cr_2O_3) which performs as a coherent barrier against corrosion (Ghahremaninezhad and Wang, 2012). Nevertheless, various iron oxides and iron oxy-hydroxides are formed on the carbon steel surface which may have protective structures performing as diffusion barrier. The formation of various oxides and oxy-hydroxides is strongly

affected by concentration of oxygen and hydrogen ions, humid and dry environment conditions, electrochemical potential, dissolved ions in aqueous solution, and thermodynamic stability of the oxides and oxy-hydroxides (Waseda and Suzuki, 2005; Zise *et al*., 2007; Takahashi *et al*., 2005).

1.2 Knowledge Gap

Several modeling and numerical studies have been done on the crevice corrosion behaviour of stainless steel including concentration and pH profile, corrosion current profile, and mass transport mechanism of dissolved species within the crevice (Heppner *et al.*, 2004; Kennell *et al.*, 2008; Kennell and Evitts, 2009). These studies have focused on the behaviour of corroding crevice in different distances from the crevice mouth. Moreover, many experimental studies have been conducted on monitoring electrochemical processes within engineered crevices. Combination microelectrodes were used at different positions within the engineered crevice to detect and record the potential, pH and chloride ions concentration simultaneously (Yan *et al*., 2007; Wolfe *et al*., 2004; Wang *et al*., 2014). In spite of different numerical and experimental studies on the chemical conditions at different positions within the engineered crevices, there are only few experimental studies on the corrosion mechanism of the carbon steel in chloride containing environments. In addition, there is insufficient knowledge on the crevice corrosion behaviour of carbon steel in acidic solutions containing chloride ions. Hue et al., (2010) investigated the crevice corrosion of carbon steel with engineered crevice in alkaline solution in the presence of chloride ion.

1.3 Thesis Objectives

The overall aim of this MSc project was to examine the corrosion behaviour of carbon steel under disbonded coating and determine the composition of corrosion products formed on

carbon steel surface in sulphuric acid solution in the presence of chloride and iron (III) ions. Five major objectives were defined to complete this research project:

1. To determine the type of the corrosion on the carbon steel surface with engineered crevice gap, perform immersion tests at various temperatures and concentrations.
2. To investigate the morphology of the corrosion products layer formed on the surface of carbon steel after immersion in solutions with different concentrations of chemicals by conducting SEM analysis.
3. To investigate the phase composition of the corrosion products layer by conducting XRD analysis and investigate formation of protective and non-protective layers on the steel surface.
4. To identify the mechanism of corrosion and associated electrochemical reactions using XRD analysis and potentiodynamic test.
5. To identify any corrosion stages and current-potential changes by conducting electrochemical noise measurement tests.

1.4 Thesis Structure

The thesis is divided into 6 chapters. Chapter one presents a background of the material that will be discussed throughout the thesis. Also, the knowledge gap resulting in present work as well as objectives of this research are explained in the following sections of this chapter. Chapter two gives a brief literature review on the uranium extraction process, rubber lining, corrosion behaviour of carbon steel, and corrosion measurement techniques employed to complete the objectives of this research.

Chapter three discusses objectives 1 and 2 of this research. The materials and methods used to accomplish these tasks, the results and discussion of immersion test and SEM analysis, and summary and conclusions are given in this chapter. Chapter four explains the materials and methods of objective 3 and objective 4. The results of the XRD and potentiodynamic test are presented and discussed, and finally the summary and conclusions of the analysis and measurement are explained. Chapter five discusses the materials and methods employed to complete the last objective of this research. The results of the ECN test for carbon steel and austenitic stainless steel are presented, and the results are discussed. A summary of the test and results as well as conclusions are given at the end of this chapter. The last chapter covers a summary of the conclusions, recommendations and suggestions for future studies.

Chapter Two

2 Literature Review

2.1 Uranium Extraction

Uranium is extracted from its ore through hydrometallurgical processes including leaching, solvent extraction and precipitation. Uranium ores vary from deposit to deposit based on their grades and sources; nevertheless, the extraction process is almost identical for most of them. The basic steps of a general uranium extraction process consist of crushing and grinding, leaching, solid-liquid separation and washing, solvent extraction and yellow cake precipitation and drying. Most uranium mills use wet grinding so that a slurry product is fed to the leaching solution which contains an acid or base as well as an oxidant. The operating temperature in the leaching circuit is between 40 to 60ºC (Seidel, 1981). There are two main leaching technologies to treat the uranium ores including acid and alkaline leaching. Parameters used to determine whether acid or alkaline leaching is employed include ore carbonate content, quality requirements, environmental considerations and energy consumption (Yousif, 2006). For uranium ores with carbonate content of higher than 12% (Wt/Wt) alkaline leaching is recommended, and acid leaching is recommended for the uranium ores with less than 12% of carbonate content. The acid leaching method is usually preferred (International mining, 2008)

due to lower required temperature, energy saving and shorter duration of the leaching process (Bragadireanu *et al*., 2002).

2.2 Acid Leaching of the Uranium Extraction Process

The leaching process performs as a liquid-solid extraction process which involves a mixture of solute (desired component), solvent and solid phase. The solid phase is inert and not dissolved in the solvent phase while the solute phase is completely soluble in the solvent phase (Henley, 1981). The solute phase leaches from the solid phase into the solvent, which causes separation of the solute and solid phase. In the uranium leaching process, the uranium ore is in the solid phase, and uranium is in the solute phase which is dissolved in sulphuric acid as the solvent. Uranium is in a reduced or tetravalent form (UO_2) in most ores. Since the reduced uranium is not soluble in both acid and alkaline leaching solutions, the oxidant is used to convert the reduced uranium to a hexavalent form (UO_2^{2+}) which is completely soluble in the leaching solution (Seidel, 1981). The principle oxidant in the acid leaching is iron (III) ion (Fe^{3+}). It is usually present in the leaching solution from the solution recycle streams; however, it can be added to the solution in form of iron (III) or iron (II) sulphate or steel alloy. The iron (III) ion performs as an electron carrier and facilitates the leaching process as follows:

$$UO_{2\,(s)} + 2Fe^{3+}{}_{(aq)} \rightarrow UO_2^{2+}{}_{(aq)} + 2Fe^{2+}{}_{(aq)} \qquad (2.1)$$

A subsequent oxidant is then added to regenerate iron (II) ions to iron (III) ions so that the iron (III) ions are recovered to maintain the uranium dissolution. Various oxidants such as manganese dioxide, sodium chlorate, hydrogen peroxide and sulphur dioxide are used in the uranium acid leaching. Sodium chlorate ($NaClO_3$) is traditionally used in North America as the first option and oxidizes the iron (II) ions as follows:

$$NaClO_{3\,(s)} + 6Fe^{2+}{}_{(aq)} + 6H^{+}{}_{(aq)} \rightarrow NaCl_{\,(s)} + 6Fe^{3+}{}_{(aq)} + 3H_2O_{\,(l)} \quad (2.2)$$

Reaction (2.2) shows that the chloride ions are released by oxidation of iron (II) ions. These chloride ions are dangerous and cause corrosion of construction materials (Venter and Boylett, 2009). Miki and Nicol, (2009) studied the kinetics of the oxidation of iron (II) ions by sodium chlorate in the leaching circuit of the uranium ores. They concluded that rapid reduction of chlorate ions demonstrates that the sodium chlorate cannot be the actual oxidant for tetravalent uranium.

1 to 3% of sulphuric acid is used in the leach solution to form soluble uranyl sulphate complexes (UO_2SO_4, $[UO_2(SO_4)_2]^{2-}$, $[UO_2(SO_4)_3]^{4-}$). This concentration represents a very dilute sulphuric acid which is significantly corrosive for metals and alloys especially carbon steels. Panossian *et al*., (2012) did a review on the corrosion of carbon steel pipes and tanks by concentrated sulphuric acid. According to this review, the corrosion rate of carbon steel in dilute sulphuric acid solutions is a function of its chemical composition, especially the carbon content. In dilute sulphuric acid solutions up to 50% (g l^{-1}), the corrosion rate increases with increasing the sulphuric acid concentration. Also, the corrosion rate increases as the carbon content increases. In contrast, above a concentration of 50%, the corrosion rate decreases for all carbon steels with different carbon contents. Finally, at concentrations higher than approximately 63%, the corrosion rate is very low and almost the same for all carbon steels demonstrating the independence of the corrosion rate from carbon content. This trend is attributed to the formation of a dark gray protective layer of iron (II) sulphate on the carbon steel surface in concentrated sulphuric acid solutions according to the reaction (2.3):

$$H_2SO_{4\,(l)} + Fe_{\,(s)} \rightarrow FeSO_{4\,(s)} + H_{2\,(g)}\uparrow \quad (2.3)$$

2.3 Rubber Lining

Elastomeric linings referred to as rubbers are bonded to the steel substrates and used to protect steel process vessels. Failure of the rubber lining can occur due to the chemical action and or mechanical damage. Absorption of the medium through the rubber results in swelling of the rubber coating and further chemical deterioration. Rubbers absorb materials they are in contact with, and this absorption can cause swelling, cracking and penetration to the steel substrate of the rubber lined process vessels and finally failure of the bond. Chemical deterioration can also happen due the reaction of the medium and the rubber coating. It increases with increasing the solution concentration and temperature (Schweitzer, 2007).

2.4 Corrosion Behaviour of Carbon Steel

2.4.1 Characteristics of Corrosion Products on Carbon Steel Surface

Corrosion products formed on a carbon steel surface mainly consist of various iron oxides, iron hydroxides, and iron oxy-hydroxides. The morphology and phase composition of the corrosion products are important since the corrosion rate and properties of substrates are strongly affected by the characterization of the corrosion products layer. The corrosion process of iron in aqueous solutions includes re-oxidation and reduction of iron (II) and iron (III) ions. The iron is dissolved as iron (II) ions into the solution, and these ions are precipitated onto the metal surface as the corrosion products layer (Waseda and Suzuki, 2005).

Zise *et al*., (2007) studied the morphology and phase composition of the corrosion product on cast iron (3% carbon content) in 0.06 M NaCl+ 0.03 M Na_2SO_4+ 0.01 M $NaHCO_3$ de-oxygenated solution. They immersed specimens at the bottom of beaker for 48 and 138 days,

and performed SEM and XRD analyses after immersion time. The SEM and XRD analyses of the specimens immersed for 48 days indicated that the corrosion products of the upper surface were goethite (α-FeOOH) with grain-like shape. However, the corrosion products on the beneath surface were mainly lepidocrocite (γ-FeOOH) with leprose or petal-like appearance. Surface analysis of the specimens immersed for 138 days showed that three layers of corrosion products covered the surface of the specimens. The inner layer was made up of goethite, magnetite (Fe_3O_4) and a little akaganeite (β-FeOOH). The middle and outer layers were made up of lepidocrocite and goethite (stalactite shape) respectively. α-FeOOH with stalactite shape has compact and continuous structure which helps protect iron matrix against further corrosion attacks. However, γ-FeOOH decomposes to Fe^{3+} in acid environments accelerating iron corrosion as follows:

$$\gamma\text{-FeOOH}_{(s)} + 3H^{+}_{(aq)} \rightarrow Fe^{3+}_{(aq)} + 2H_2O_{(l)} \quad (2.4)$$

Moreover, a high concentration of chloride ions causes the formation of akaganeite (β-FeOOH) with an acicular shape structure. Akaganeite is formed between the corrosion products layer and iron substrate with action of chloride ions in a humid environment in the presence of oxygen and water. The chloride ions, present in the akaganeite lattice, can accelerate the iron by releasing in ionic form and dissolving in the acid solution. They concluded that the iron oxides are more stable and protective than the iron oxy-hydroxides due to the compact and regular structure and lower free energy of formation of the lattice.

Takahashi *et al*., (2005) studied the corrosion products constituents formed on the pure iron specimens conducting in-situ x-ray diffraction measurements. They dropped 2% NaCl solution and 2% Na_2SO_4 solution onto the surface of the specimens, and maintained them for

1000 hours in a humid atmosphere at ambient temperature. They carried out the XRD before and after drying process. The results of the humid condition tests for both solutions showed that γ-FeOOH was the main constituent of the corrosion products with fractions of other corrosion products. For the dry condition, the intensity of α-FeOOH diffraction peaks, formed in 2% NaCl, were increased relative to the humid condition. However, the composition of the corrosion products, which formed in 2% Na_2SO_4 solution, did not change in the dry condition demonstrating that different factors affect the iron corrosion process including the humid and dry condition, anions present in the solution, and concentration of dissolved oxygen and hydrogen ion.

2.4.2 Crevice Corrosion Behaviour of Carbon Steel

Crevice corrosion is a localized attack in acid-chloride conditions occurring in prone regions of metals and alloys like under deposits, beneath gaskets, in imperfect welding, interface of washers, and within pits and cracks. Crevice corrosion affects metals and alloys that form a protective thin oxide layers on their surface. A small current called the passive current, can pass through the protective film since the film does not have a high electrical conductivity. Therefore, in the presence of the protective film, metal dissolution occurs at a very slow rate. However, in concentrated acid-chloride solutions, the protective film is destroyed when the solution pH and chloride concentration reach a critical state that is called the critical crevice solution (Heppner, 2006; Evitts, 1997). Crevice corrosion develops because of the difference in inside and outside solution including differential aeration, pH, metal ion concentration and chloride ion concentration (Malik *et al*., 2001).

The mechanism of the crevice corrosion falls into three stages of incubation, initiation and crevice corrosion development. The crevice moves to the initiation stage as the protective film is completely destroyed; however, it remains in the incubation stage and does not enter to the initiation stage if the protective film is not destroyed. During the incubation period, due to the geometry of the crevice, oxygen may diffuse at a lower rate than it is consumed within the crevice, and oxygen depletion occurs (Kennell *et al*., 2008). The depletion of oxygen within the crevice causes cathodic reactions to occur outside the crevice on the bold surface and accelerated anodic dissolution of iron and further hydrolysis of dissolved iron in the crevice. The hydrolysis of dissolved iron acidifies the crevice. The high concentrations of chloride ions as well as hydrogen ions released from hydrolysis of dissolved iron attack the protective film and may destroy it so that crevice corrosion enters to the initiation state (Kennell and Evitts, 2009).

Oldfield and Sutton, (1978) described a theory for crevice corrosion initiation of stainless steels considering a differential change of the environment in crevice. According to this theory the mechanism of the crevice corrosion falls into four stages: (1) deoxygenation, (2) increase of salt and acid concentration, (3) depassivation, (4) propagation. The disruption of protective film increases the passive current and can cause a potential drop and higher rate of corrosion in some regions within the crevice. These regions are in the crevice corrosion development stage.

Hue *et al*., (2010) studied the crevice corrosion stages of Q235 carbon steel in sodium bicarbonate ($NaHCO_3$) solution containing chloride ion using the electrochemical noise technique. The electrochemical cell for the EN measurements consisted of a reference electrode (RE) and two working electrodes (WE1 and WE2). The first working electrode (WE1) was carbon steel with an engineered crevice with a working area of 0.1 cm^2, and the second one (WE2) was a plane carbon steel without an engineered crevice and three different working areas

of 0.1 cm^2, 1 cm^2 and 16 cm^2. The carbon steel surface was sealed with insulating tape in order to create a crevice gap with an exposed area of 0.1 cm^2. They performed EN test for three different r values of 1, 10 and 16 where r was the area ratio of WE2 to the crevice area of WE1.

The results showed that in the first few hours, current noise (Ig) was very small and potential (E) was positive which indicated that the crevice corrosion was not developed yet due to the passivation of WEs. However, after few hours, the potential shifted toward negative points, and a significant decrease in potential and a large increase in current were observed. This demonstrated that the passive film on the WE1 was destroyed, and the crevice corrosion was in transpassive region where the active dissolution of metals occurs. After about 4 hour, the current noise decreased significantly, and the potential decreased simultaneously. Then, the potential and current only fluctuated slightly without significant changes. In this period, the crevice corrosion enters into a stable state in which the corrosion rate is low. Differences were observed in the results for different r values and showed that the induction period increased with r. Moreover, the area ratio had a remarkable effect on development of the crevice corrosion. They concluded that for small r values, potential difference between inner and outer crevice surface is small, and the outer crevice surface is in the active dissolution stage. Therefore, crevice corrosion is not greatly accelerated within the crevice. On the contrary, for large r values, the outer surface is in the passive state, and degree of acceleration is high within the crevice.

Different factors influence the crevice corrosion occurrence including the crevice and bold surface geometries, protective film, mass transport of dissolved species inside and outside the crevice, electrochemical reactions, and bulk solution composition (Betts and Boulton, 1993). Fig. 2.1 shows a schematic diagram of crevice corrosion with possible electrochemical reactions.

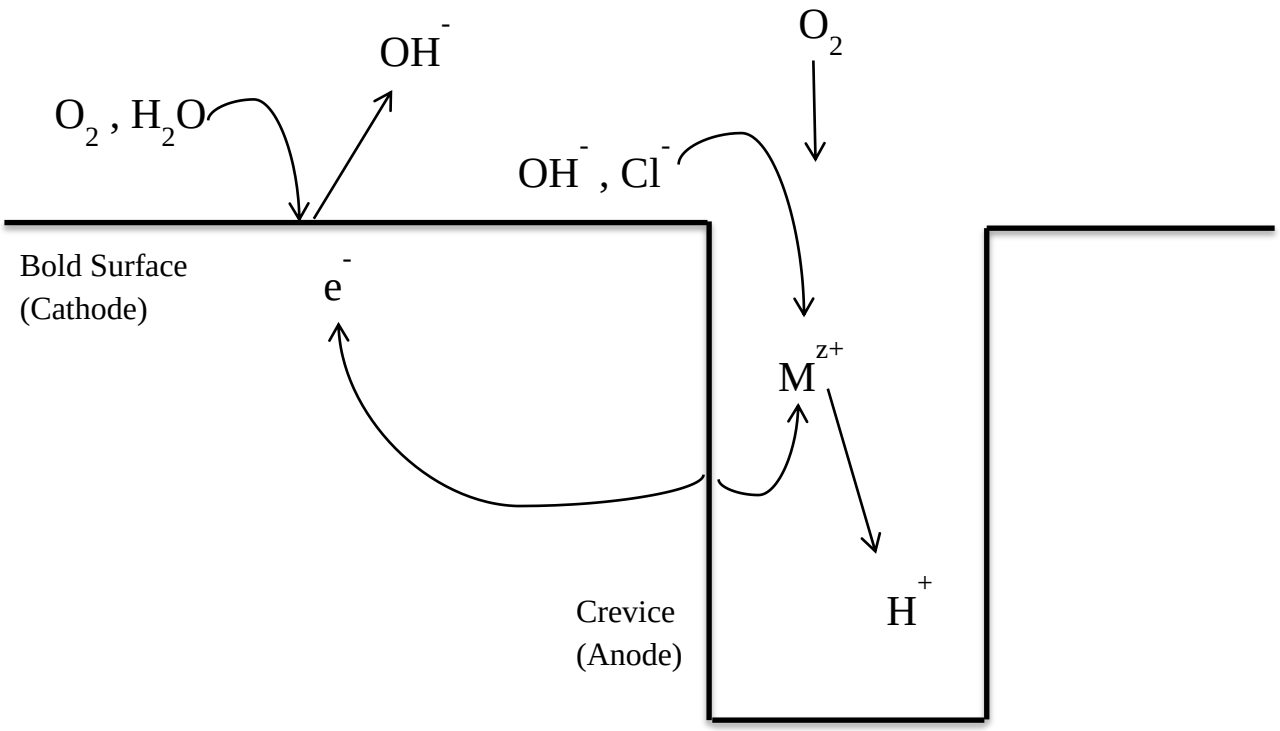

Fig. 2.1. Schematic diagram of crevice corrosion (Kennell and Evitts, 2009)

2.4.3 Pitting Corrosion Behaviour of Carbon Steel

Pitting corrosion happens at the metal surface covered with the passive or protective layer (a thin oxide layer) during the access of aggressive anions, especially chloride ions. A critical potential called the pitting potential (E_p) must be exceeded for the initiation of pitting corrosion. According to equation (2.1), pitting potential decreases as the aggressive anion concentration increases (Marcus, 2002).

$$E_p = a - b \log [A] \quad (2.1)$$

Where, A is the anion concentration.

Based on the composition of metals and alloys and environmental conditions, the mechanism of pit growth may be different. However, there is a general mechanism including breakdown of passivity, pit growth and repassivation phenomena (Jones, 1996). Three main mechanisms for passive film breakdown are found in the literature (Marcus, 2002):

1. The penetration mechanism: Penetration occurs due to the action of chloride ions incorporated in oxide ions (O^{2-}) which are called cation vacancies. These cation vacancies migrate from the oxide surface to the metal surface with a rate equivalent to the transport of cations from the metal to oxide surface. Accumulation happens at the interface of the metal and oxide layer if the cation vacancies penetrate into the metal or alloy phase at a slower rate than their transport through the passive layer. This accumulation results in local concentration causing stresses within the passive layer and breakdown of passivity.
2. The film breaking mechanism: Any sudden changes of the electrode potential or chemical changes of the surface cause negative stress within the passive layer. These changes lead to release of metal ions into the electrolyte and eventually film breakage. Moreover, existence of any crack within the passive layer in presence of chloride ions causes direct contact of the crack area of the metal surface with the aggressive chloride ions and pit formation.
3. The adsorption mechanism: In the adsorption mechanism, chloride ions are adsorbed at the interface of the oxide layer and electrolyte and enhance the transport of the metal cations from the oxide layer to the electrolyte. This process causes thinning of the passive layer and may lead to its total removal. Halide ions like chloride ions have tendency to make complexes with the metal cations and decrease their charge. The reduced forms of

the metal ions require less activation energy to migrate into the electrolyte. This anodic dissolution of metal cations stabilizes the pitting corrosion and prevents repassivation of the damaged sites within the passive layer.

Studies base on experimental results have shown that the film breaking and adsorption mechanisms are more probable than the penetration mechanism. The passivity breakdown causes the pits which are deposited on inert substrates pass through the layers in a few seconds. They then grow outwards perpendicular to the inner substrates with increasing their radius. During the pit growth an active anode which is the pit and a passive cathode, which is the passive layer around the pit, will be created. In a slightly alkaline chloride containing solution dissolved metal ions (Me^{2+}) are hydrolyzed according to reaction (2.5):

$$Me^{2+} + 2H_2O \rightarrow MeOH^{+} + H_3O^{+} \quad (2.5)$$

For stainless steels, Me^{2+} denotes iron ions; however, there are additional anodic dissolution reactions for nickel and chromium which are similar to the iron reaction. The hydrolysis of the metal ions drops the pH and causes migration of the chloride ions into the pit. The chloride ions, migrating to the pit, causes formation of a porous cap at the pit mouth and produce aggressive hydrochloride acid solution as follows:

$$Fe^{2+} + 2H_2O + 2Cl^{-} \rightarrow Fe(OH)_2 + 2HCl \quad (2.6)$$

In some cases pitting corrosion stops if a new oxide film forms on the surface of the metal or alloy. However, it will propagate if the corrosive environment contains a high chloride ion concentration so that the repassivation is impossible (Jones, 1996). Fig. 2.2 shows a schematic diagram of pitting corrosion occurring on the iron substrate.

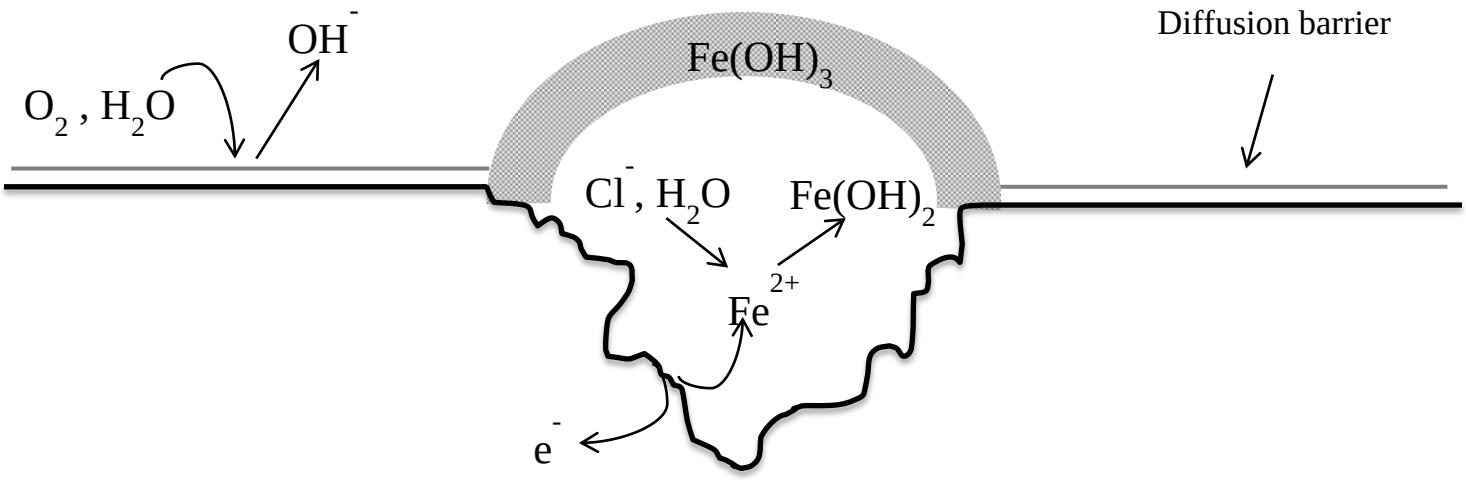

Fig. 2.2. Schematic diagram of pit growth on the iron substrate (Jones, 1996)

2.5 Corrosion Measurement Techniques

Several corrosion measurement tests are employed to study the corrosion processes and corrosion characteristics of various metals and alloys in aqueous environments. They provide important information on the corrosion rate, corrosion mechanism, passivity and coatings by measuring the potential-current relations under certain conditions. This section explains the theories of the corrosion techniques, which were employed in this research project.

2.5.1 Electrochemical Noise Measurements

Electrochemical noise measurement is a novel technique that produces results that complement electrochemical impedance spectroscopy and linear polarization resistance test. It is defined as the spontaneous fluctuation in the current going through the metal-electrolyte interface or the fluctuation in potential applied to a corroding metal under potentiostatic or galvanostatic control.

Electrochemical noise measurement provides significant information about the rate and mechanism of the corrosion processes occurring at the electrodes interface by analysis of the potential and current fluctuations (Loto, 2012). The corrosion reactions show small current fluctuations of μA to mA and small potential fluctuations of μV to mV since the corrosion processes always occur at low frequencies of less than 1 Hz (Perdomo and Singh, 2002).

One of the major sources of electrochemical noise is the initiation of pitting corrosion. In this technique, the corrosion reactions are monitored on two working electrodes coupled through a zero resistance ammeter (ZRA) without any external applied potential. ZRA measures the current between these two electrodes which have slightly different potentials. The potential is measured between the coupled working electrodes and a reference electrode. The electrochemical noise measurements together with some other electrochemical techniques like linear polarization resistance and electrochemical impedance spectroscopy have given remarkable information on corrosion mechanisms (Wang, 2005).

2.5.2 Potentiodynamic Measurements

Electrochemical corrosion experiments measure or control the potential and current of the reactions. Several types of methods are available to determine corrosion behaviour of metals. In the potentiodynamic technique, the applied potential (with a constant potential sweep or scan rate) is increased with time, and the current is constantly monitored. Data gained from the test are represented in a plot of potential versus logarithm of current or current density which is called polarization curve (Etor, 2009) as shown in Fig. 2.3. It is also possible to control and change the current and measure the potential. In the galvanodynamic or galvanostatic technique, the current is imposed on the electrode and the potential is measured.

Polarization curves provide useful information on the corrosion process taking place on the metal surface, including the corrosion rate, corrosion potential, Tafel slopes and polarization resistance. Furthermore, Polarization curves can determine the passive behaviour of metals and alloys. Passivity is a formation of very thin, protective oxide layer on the surface of a metal or alloy causing a high anodic polarization. As the passive layer begins to form, the corrosion rate is reduced (Jones, 1996).

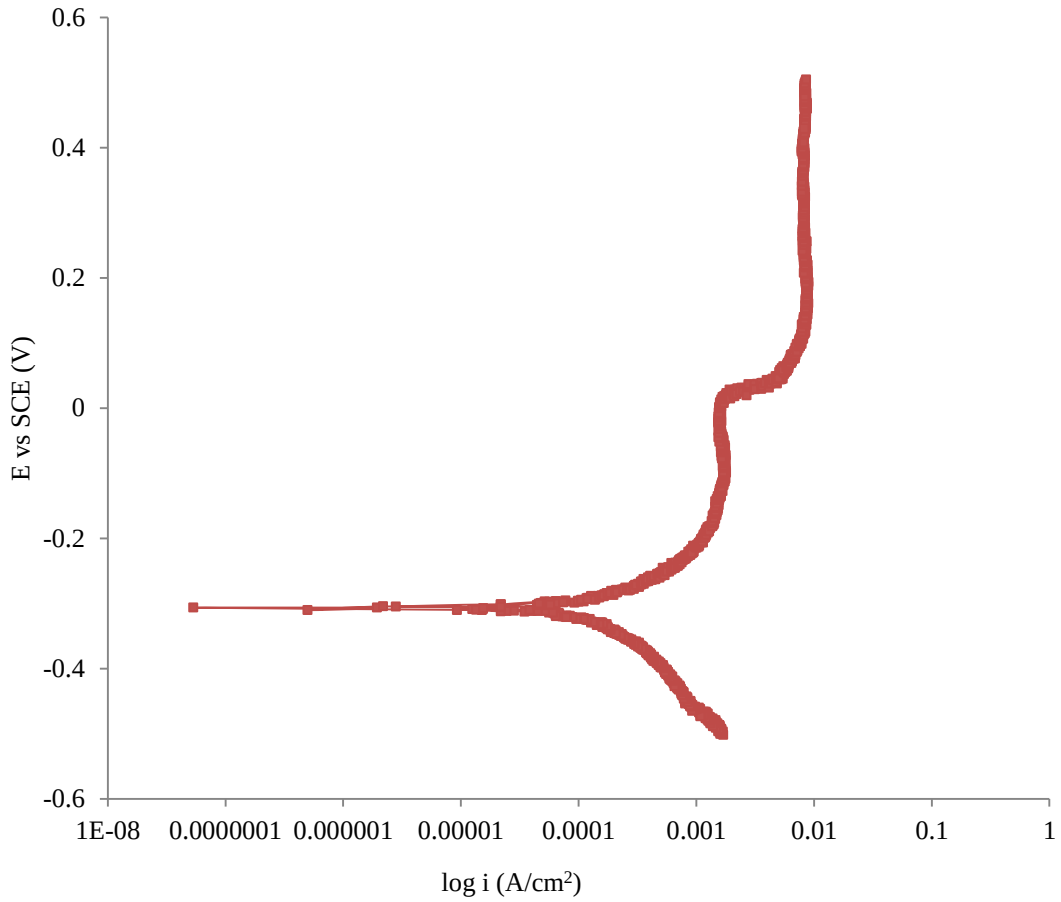

Fig. 2.3. Polarization curve of novel alloy in 3% NaCl solution

Chapter Three

3 Corrosion Type and Morphology of the Corrosion Products

3.1 Overview of Chapter 3

Chapter 3 of this thesis covers the first and second objectives of this research project. Immersion tests were conducted in certain conditions, and SEM analyses were performed on selected regions of corroded surface of the coupons to complete these objectives. The type of the corrosion taking place under disbonded coating was identified from visual observations and the SEM analysis. Moreover, the morphology of the corrosion products layer was investigated from the SEM results.

3.2 Experimental Procedure

3.2.1 Sample Preparation

Carbon steel coupons with dimensions of 7.5 cm x 7.5 cm x 0.6 cm were cut from A36 carbon steel plates. Table 3.1 shows the chemical composition (Wt%) of the alloy. The under surface and edges of the carbon steel coupons were coated with enamel paint leaving exposed areas of 26 cm^2 with dimensions of 6.5 cm x 4 cm. Fig. 3.1 shows a carbon steel coupon coated with enamel paint. The exposed surfaces of the coupons were polished with 400 and 600 grit

sand paper and rinsed with RO water and acetone. The engineered disbonded coatings, with dimensions of 7.5 cm x 7.5 cm x 0.6 cm, were cut from an acrylic sheet. Also, acrylic spacer sheets with dimensions of 7.5 cm x 3 cm x 0.1 cm were cut and placed between the carbon steel coupons and acrylic coatings to form the engineered crevices with thickness of 1 mm. Fig. 3.2 shows a schematic diagram of experimental setup for the immersion test. The carbon steel coupons with engineered crevices were immersed in 10 g l^{-1} and 50 g l^{-1} of H_2SO_4 solutions containing 1 g l^{-1} and 3 g l^{-1} of NaCl and 3 g l^{-1} of $Fe_2(SO_4)_3$ for 14 days. The concentration of chemicals was chosen according to the uranium leaching process characteristics. Table 3.2 shows the concentration of chemicals in three different solutions.

Table 3.1. Chemical composition of A36 carbon steel

Component	C	Cu	Mn	P	Si	S	Fe
Wt %	0.25	0.2	1.03	0.04	0.28	0.05	98

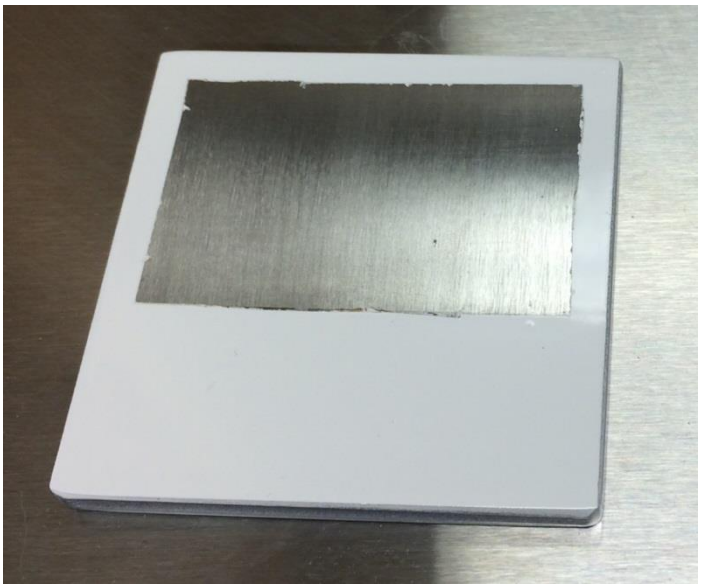

Fig. 3.1. Carbon steel coupon coated with enamel paint

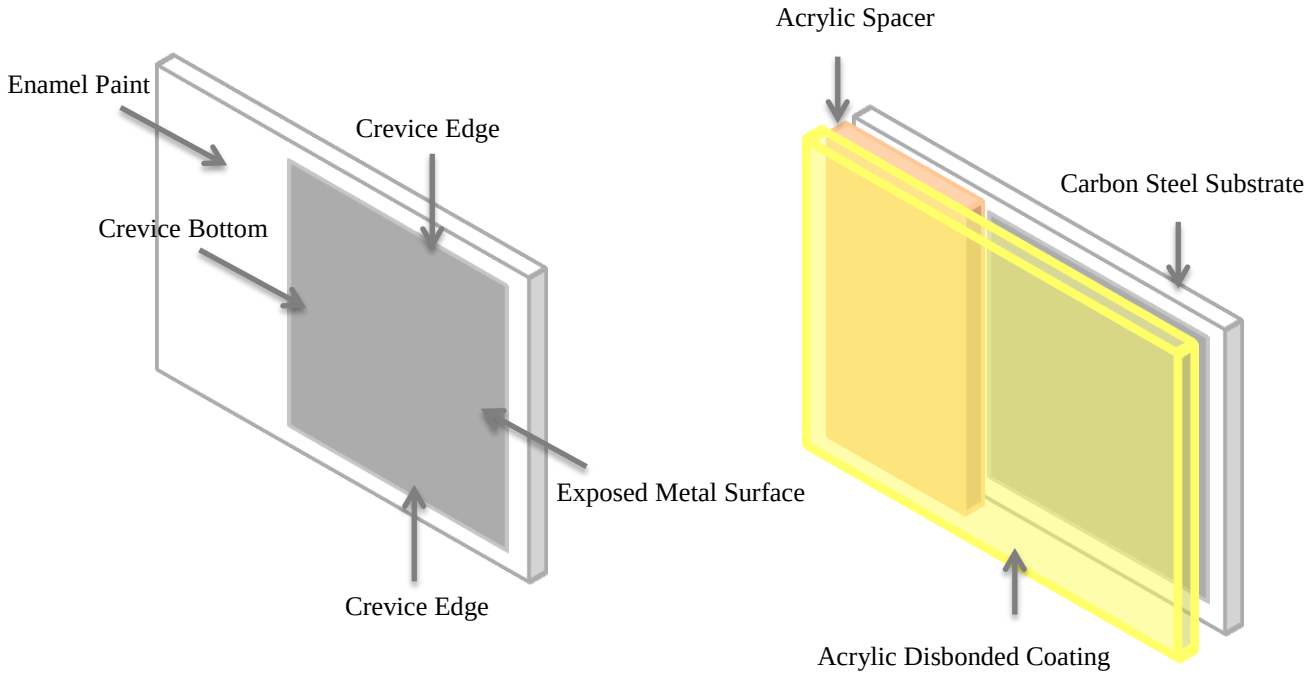

Fig. 3.2. Schematic diagram of carbon steel coupon with the engineered disbonded coating

Table 3.2. Chemicals concentrations in different solutions

Chemicals / Conc. (g l^{-1})	Solution 1	Solution 2	Solution 3
H_2SO_4 (Fisher Scientific, USA)	10	50	50
NaCl (Fisher Scientific, USA)	1	1	3
$Fe_2(SO_4)_3$ (Sigma-Aldrich, USA)	3	3	3

3.2.2 Solution Preparation

The solutions used for the immersion test were 500 ml of 5 g H_2SO_4 + 0.5 g NaCl + 1.5 g $Fe_2(SO_4)_3$ with pH of 1.85, 500 ml of 25 g H_2SO_4 + 0.5 g NaCl + 1.5 g $Fe_2(SO_4)_3$ with pH of 1.4, and 500 ml of 25 g H_2SO_4 + 0.5 g NaCl + 1.5 g $Fe_2(SO_4)_3$ with pH of 1.4. All solutions were prepared using RO water. The temperature was controlled at 55 ± 0.1°C, which is the leach

solution temperature, using a digital immersion circulator. Beakers that contained the immersed coupons were placed in a reservoir containing water. The immersion circulator was installed at the corner of the reservoir so that heater coil of circulator was fully immersed in the water bath. The mouths of the beakers were covered with plastic wraps to prevent evaporation of the solution. A clear plastic tube was placed at the mouth of each beaker allowing diffusion of atmosphere oxygen into the solution.

3.2.3 SEM Device Characteristics

The corrosion coupons were taken out after 14 days of immersion, and the SEM analysis was conducted immediately after immersion test. A Hitachi SU6600 field emission gun scanning electron microscope was employed to conduct the SEM analysis on the corroded surfaces of the coupons. The electron microscope operated at voltage of 20 kV.

3.3 Surface Morphology Analysis, Results and Discussion

The SEM analysis of the corrosion product layers formed on the carbon steel surface was carried out after 14 days of exposure. Fig. 3.3 shows the SEM images of the corrosion products layer for selected areas of the coupons. Visual observations and the SEM analysis showed that several pits were formed on the carbon steel coupons under the disbonded coatings. Formation of the pits on the substrate indicated disruption of the continuous layer of the corrosion products, which was formed over the substrate surface.

It is shown that the size of the pits, which were formed in the solution of 10 g l^{-1} H_2SO_4, 1 g l^{-1} NaCl, 3 g l^{-1} $Fe_2(SO_4)_3$, are small (Fig. 3.3. a). The size of the pits increased as the sulphuric acid concentration increased from 10 g l^{-1} to 50 g l^{-1} (Fig. 3.3. b). However, they did not increase

significantly as the concentration of sodium chloride was increased from 1 g l^{-1} to 3 g l^{-1} (Fig. 3.3. c). In spite of that, the structures of the corrosion products within the pits were more porous for 3 g l^{-1} of sodium chloride. This indicates that corrosion rate of carbon steel under the disbonded coating is related to the sulphuric acid and sodium chloride concentration. Therefore, the higher solution concentrations result in greater corrosion rates due to the increased activity of dissolved species including sulphate (SO_4^{2-}) and chloride (Cl^-) ions (Loto, 2013). The presence of SO_4^{2-} together with the Cl^- ions creates an aggressive solution that favours pit formation.

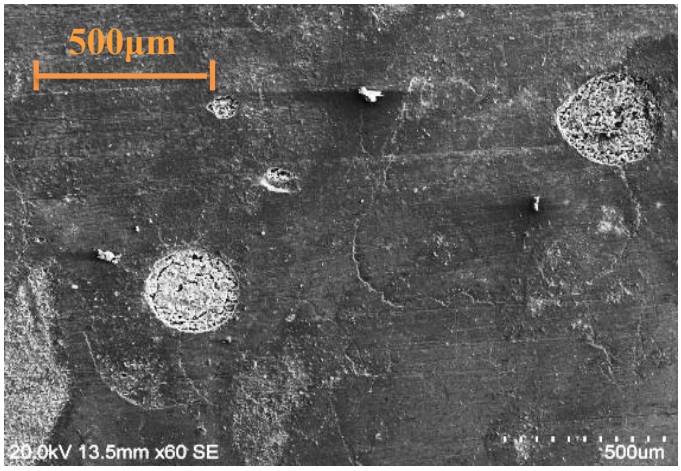

(a) Solution 1: 10 g l^{-1} H_2SO_4, 1 g l^{-1} NaCl, 3 g l^{-1} $Fe_2(SO_4)_3$

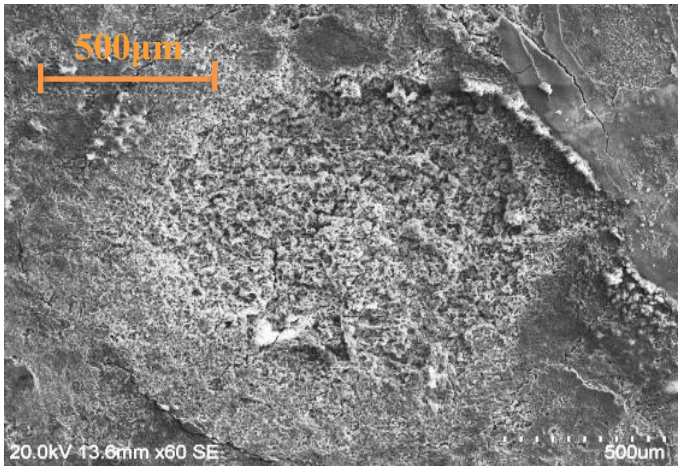

(b) Solution 2: 50 g l^{-1} H_2SO_4, 1 g l^{-1} NaCl, 3 g l^{-1} $Fe_2(SO_4)_3$

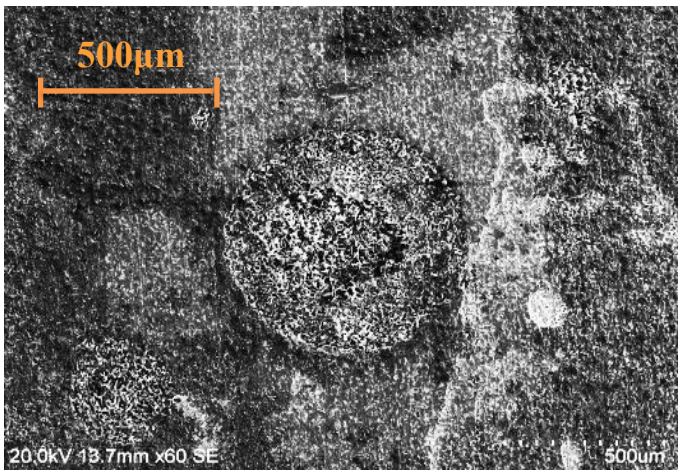

(c) Solution 3: 50 g l^{-1} H_2SO_4, 3 g l^{-1} NaCl, 3 g l^{-1} $Fe_2(SO_4)_3$

Fig. 3.3. SEM images of corrosion products layer formed on the carbon steel surface under the disbonded coating in different solutions after 14 days of immersion at 55 ± 0.1°C

Chloride ions catalyze dissolution of the diffusion barrier and liberation of Fe^{3+} in which accelerate breakdown of diffusion barrier during the initiation period of pitting corrosion as follows (Jones, 1996):

$$FeOOH + Cl^- \rightarrow FeOCl + OH^- \quad (3.1)$$

$$FeOCl + H_2O \rightarrow Fe^{3+} + Cl^- + 2OH^- \quad (3.2)$$

As the diffusion barrier is destroyed by action of the chloride ions, direct anodic dissolution of substrate occurs. The hydrolysis of the dissolved iron reduces the pH, and the reduced pH causes migration of chloride ions into the pit. The chloride ions, which migrate into the pit, develop an acid chloride condition. The acid chloride condition in the initiation sites accelerates anodic dissolution of iron causing pit propagation.

During pit propagation, a non-protective porous iron oxide layer is accumulated at the mouth of the pit (Caceres *et al*., 2009) slowing down mass transfer of dissolved iron into the bulk solution (Jones, 1996). However, the porous structure allows slow diffusion of chloride ions into the pit so that an acidic chloride solution is developed causing enhanced pitting. Chloride ions are fairly small and have high diffusivity which leads to disruption of the protective layer (Loto, 2013). Fig. 3.4 shows a schematic diagram of pitting corrosion on the carbon steel surface. It is shown that the corrosion products layer has more porous distribution inside the pit while it has a compact and continuous distribution outside the pit. Also, during the pit propagation stage, the pit performs as anode, where the active dissolution of pit occurs, and the diffusion barrier (protective layer) around the pit performs as cathode, where the cathodic reduction occurs.

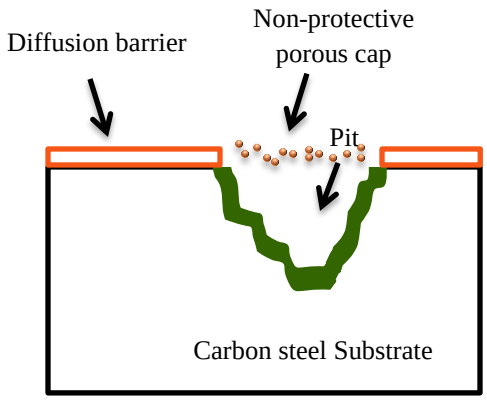

Fig. 3.4. Schematic diagram of pitting corrosion on carbon steel surface

Fig. 3.5 shows the SEM images of the corrosion products formed inside the pits after immersion in the solution of 10 g l^{-1} H_2SO_4, 1 g l^{-1} NaCl, 3 g l^{-1} $Fe_2(SO_4)_3$ at 55°C. The corrosion products formed at the pit mouth had relatively compact distributions; however, the corrosion products formed outside the pit had more compact and continuous distributions than the corrosion products formed inside the pit.

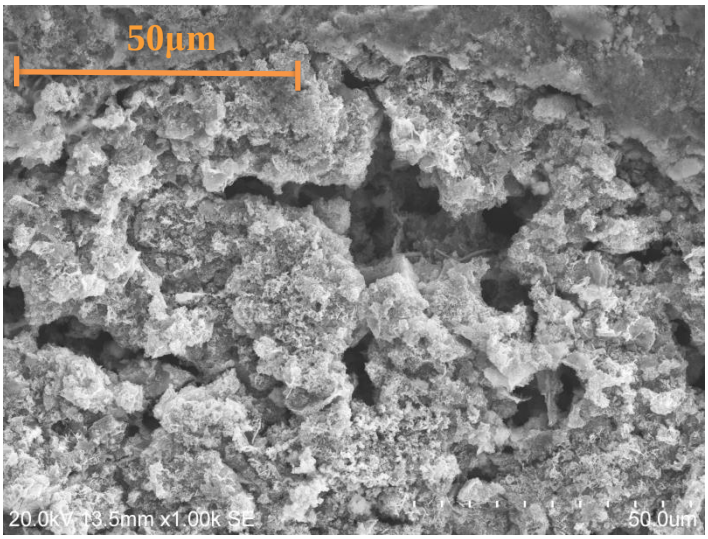

Fig. 3.5. SEM image of the corrosion products layer formed on the carbon steel surface under the disbonded coating after 14 days of immersion in a solution of 10 g l^{-1} H_2SO_4, 1 g l^{-1} NaCl, 3 g l^{-1} $Fe_2(SO_4)_3$ at 55 ± 0.1°C, inside the pit

Fig. 3.6 shows the SEM image of the corrosion products formed inside the pit after immersion in the solution of 50 g l^{-1} H_2SO_4, 1 g l^{-1} NaCl, 3 g l^{-1} $Fe_2(SO_4)_3$ at 55°C. The corrosion products distributions became more porous, loose and irregular as the concentration of sulphuric acid was increased from 10 g l^{-1} to 50 g l^{-1}. When the sodium chloride concentration increased from 1 g l^{-1} to 3 g l^{-1}, the corrosion products distributions became very loose and open (Fig. 3.7).

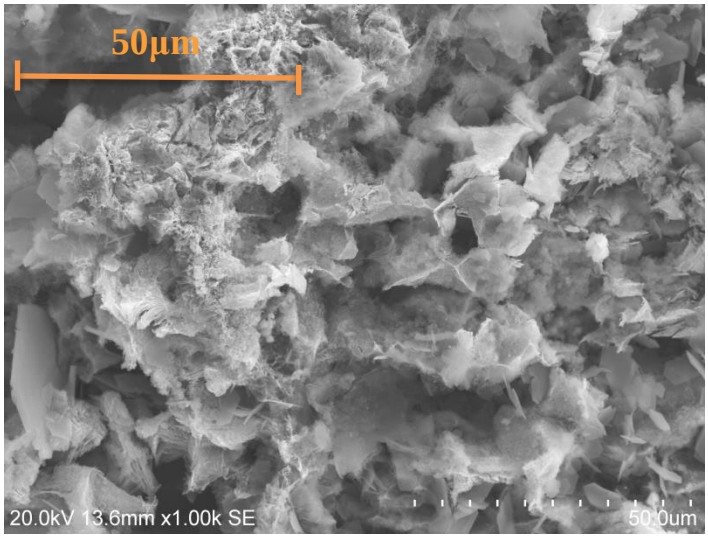

Fig. 3.6. SEM image of the corrosion products layer formed on the carbon steel surface under the disbonded coating after 14 days of immersion in a solution of 50 g l^{-1} H_2SO_4, 1 g l^{-1} NaCl, 3 g l^{-1} $Fe_2(SO_4)_3$ at 55 ± 0.1°C, inside the pit

The loose and open structure of the corrosion products, which are accumulated at the pit mouth, allows the easy access of chloride ions to the carbon steel substrate (Waseda and Suzuki, 2005) and causes corrosion acceleration. Therefore, the higher the chloride concentration, the greater corrosion rate due to either their strong attack to the protective layer or diffusion in to the pit. Moreover, the shape of the corrosion products changed at higher concentrations demonstrating that composition of corrosion products is affected by the solution concentration. Also, the change in shapes of the corrosion products indicates that various types of the corrosion products are formed on the carbon steel surface.

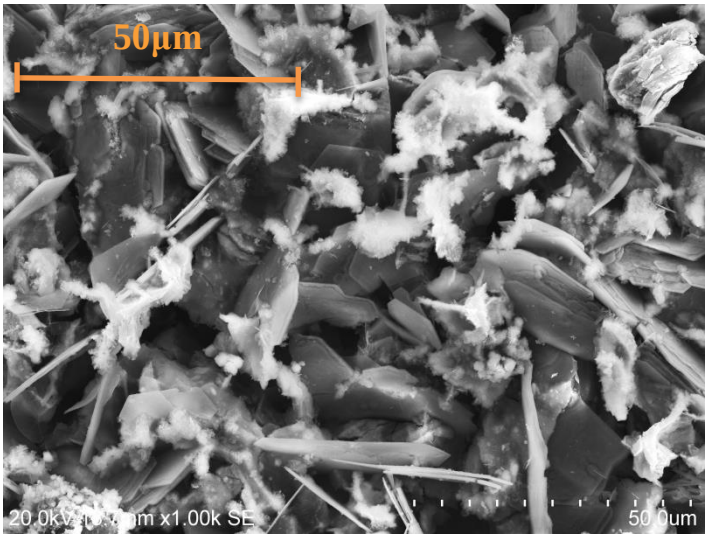

Fig. 3.7. SEM image of the corrosion products layer formed on the carbon steel surface under the disbonded coating after 14 days of immersion in a solution of 50 g l^{-1} H_2SO_4, 3 g l^{-1} NaCl, 3 g l^{-1} $Fe_2(SO_4)_3$ at 55 ± 0.1°C, inside the pit

The SEM images of the corrosion products were taken at selected areas outside the pits as shown in Fig. 3.8. The results indicated that the corrosion products formed in various solution concentrations had a very compact, close, adhesive and regular distribution. The compact corrosion product is a diffusion barrier and prevents diffusion of aggressive dissolved species onto the carbon steel surface.

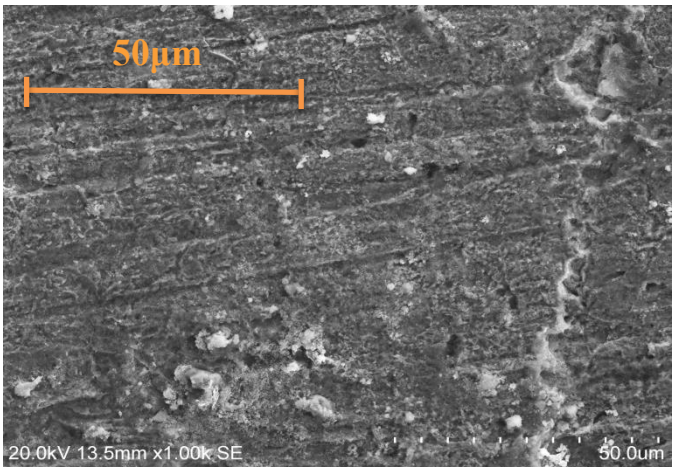

(a) Solution 1: 10 g l^{-1} H_2SO_4, 1 g l^{-1} NaCl, 3 g l^{-1} $Fe_2(SO_4)_3$

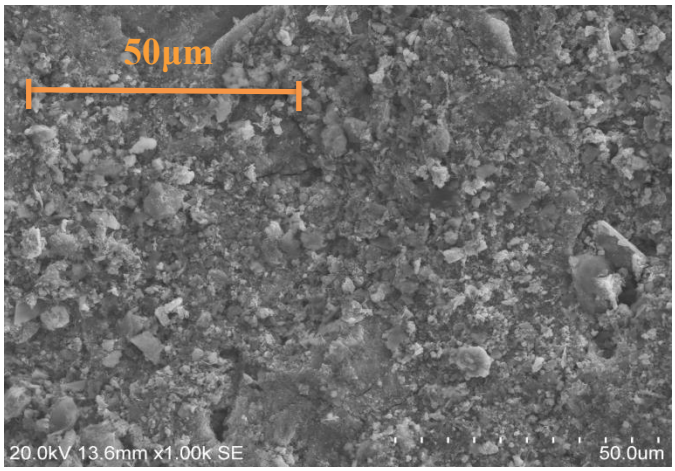

(b) Solution 2: 50 g l^{-1} H_2SO_4, 1 g l^{-1} NaCl, 3 g l^{-1} $Fe_2(SO_4)_3$

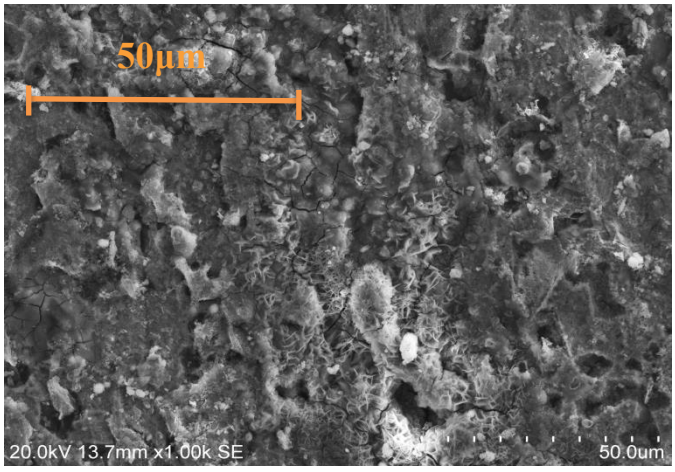

(c) Solution 3: 50 g l^{-1} H_2SO_4, 3 g l^{-1} NaCl, 3 g l^{-1} $Fe_2(SO_4)_3$

Fig. 3.8. SEM images of corrosion products layer formed on the carbon steel surface after 14 days of immersion at 55 ± 0.1°C, outside the pit

3.4 Summary and Conclusions

The type of corrosion taking place on the carbon steel surface under the disbonded coating was investigated by conducting immersion tests with several solution compositions at 55 ± 0.1°C. Also, SEM analysis was conducted at the selected areas of the carbon steel surface to investigate the morphology of the corrosion products. The following conclusions were drawn from the immersion test and SEM analysis:

1. Only general and pitting corrosion occurred on the carbon steel surface under the disbonded coating, and crevice corrosion did not occur.

2. The corrosion products formed outside the pits had a continuous, adhesive and regular structure, but they had a loose and irregular structure inside the pits allowing diffusion of corrosive species into the pit and causing further pitting corrosion development.

3. The corrosion products distribution became more porous and loose as the concentration of the sulphuric acid and sodium chloride increased.

Chapter Four

4 Phase Composition of the Corrosion Products, Corrosion Mechanism

4.1 Overview of Chapter 4

Chapter 4 of the thesis covers the third and fourth objectives of this research project. In this phase of the research, immersion tests were conducted at room temperature to form a thick layer of the corrosion products on the carbon steel coupons. X-ray diffraction (XRD) was performed on selected regions of the coupons in order to identify the phase composition of the corrosion products formed on the carbon steel surface under the disbonded coating. Also, potentiodynamic test was performed to elucidate information on the corrosion mechanism of carbon steel with engineered crevice in acidified solution containing chloride ions.

4.2 Experimental Procedure

4.2.1 Experimental Setup for Immersion Test

The carbon steel coupons, with the same dimensions of the coupons used for SEM analysis, were cut from A36 carbon steel plates. The under surface and edges of the coupons were coated with enamel paint leaving working areas of 26 cm^2. The working areas of the coupons were polished and then rinsed with RO water and acetone. The acrylic sheets with the

same dimensions of the carbon steel coupons were used to simulate the disbonded coating. The acrylic spacers with dimensions of 7.5 cm x 3 cm x 0.1 cm were placed between the coupons and disbonded coatings to form the engineered crevices with thickness of 0.1 cm. The carbon steel coupons with engineered crevices were immersed in sulphuric acid solutions containing chloride and iron (III) ions with the same concentrations that were used for SEM analysis (Table 3.2). The carbon steel coupons were immersed in several solution concentrations for 60 days at room temperature (23 ± 1°C).

4.2.2 XRD Analysis

The x-ray diffraction technique was conducted on the edge and bottom areas of the crevice (See Fig. 4.1) after the carbon steel coupons were immersed in the test solutions for 60 days at room temperature. The immersion test for the XRD analysis was conducted for an extended period, since a thick layer of the corrosion products was required for the x-ray beam sampling depth.

A Bruker D8 Discover x-ray diffractometer was employed to perform XRD analysis on the corroded surface of the coupons. The anode material was Cr Kα, and current and accelerating voltage of the x-ray generator were set to 10 mA and 10 mV respectively. Also, scan step time of 100 s was chosen for corroded surfaces with lengths of 10 mm.

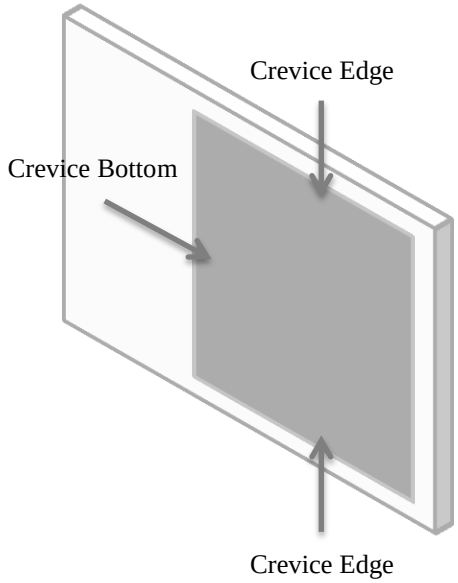

Fig. 4.1. Selected areas of the carbon steel coupons for XRD analysis

4.2.3 Potentiodynamic Scan Test

An electrochemical cell of three electrodes of a reference electrode (RE), a working electrode (WE) and a counter electrode (CE) was used to conduct the potentiodynamic scan test. Fig. 4.2 shows schematic diagrams of WEs and electrochemical cell for potentiodynamic scan test. The working electrode was a plain carbon steel coupon with dimensions of 6.5 cm x 4 cm x 0.6 cm. One surface and edges of the coupon were sealed with epoxy resin, and the other surface was left open for corrosion exposure. The exposed surface of the coupon was polished with 400 and 600 grit sand paper, and rinsed with RO water and acetone. The reference electrode was a saturated calomel electrode (SCE), and the counter electrode was a platinum electrode. The electrochemical measurements were conducted in a solution of 50 g l^{-1} H_2SO_4, 3 g l^{-1} NaCl, 3 g l^{-1} $Fe_2(SO_4)_3$ with pH of 1.4. The solution was made from analytical grade reagents and RO water.

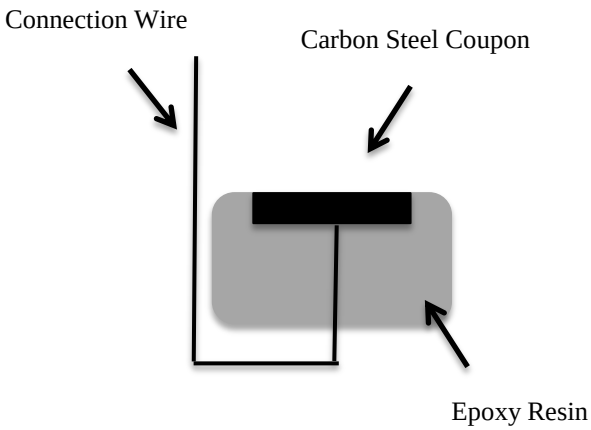

(a)

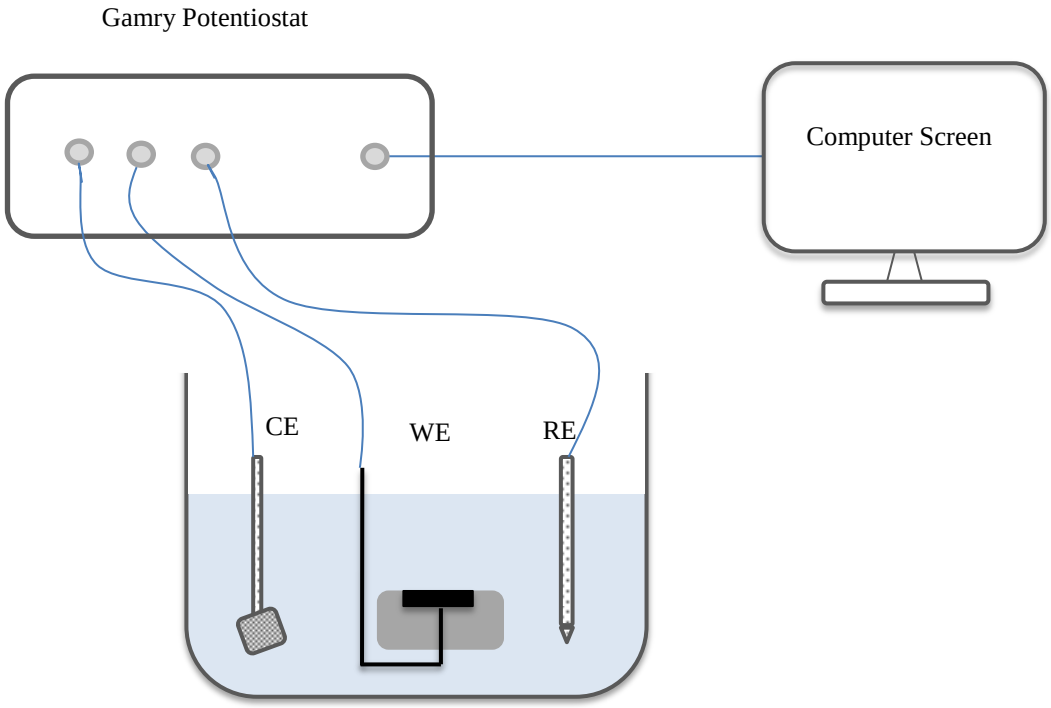

(b)

Fig. 4.2. Schematic diagram of experimental setup for potentiodynamic test, (a) WE, (b) electrochemical cell

Gamry Interface 1000™ (Gamry Instruments, USA) was used as the potentiostat device in order to carry out the potentiodynamic scan test (Fig.4.3). The Interface 1000^{TM} connects to the computer through a USB connection. It supports all Gamry electrochemical applications

software including the DC105™ DC corrosion techniques software. The DC105™ software provides users with a comprehensive set of corrosion measurement techniques. A shielded cable is connected to front panel of the Interface 1000^{TM}, and end of the cable terminates in 6 plugs with different colors that are connected to the electrochemical cell (Gamry Interface 1000^{TM} Operator's manual, 2012). Table 4.1 shows the cable terminations used for the potentiodynamic scan test. Data analysis was carried out with the Gamry Echem Analyst to evaluate the corrosion process and to calculate corrosion parameters such as polarization resistance, corrosion rate and Tafel slopes.

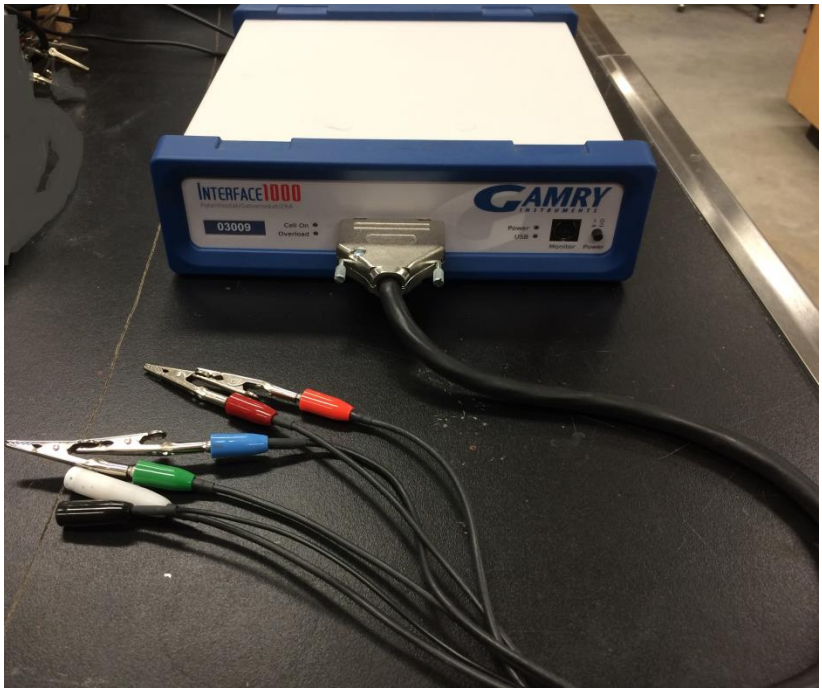

Fig. 4.3. Gamry interface 1000^{TM} employed for potentidynamic scan test

Table 4.1. Cable ends terminations for potentiodynamic scan test

Name	Color	Potentiodynamic Scan Connections
Working Electrode	Green	Connected to working electrode
Working Sense	Blue	Connected to working electrode
Counter Electrode	Red	Connected to counter electrode
Counter Sense	Orange	Connected to counter electrode
Reference	White	Connected to reference electrode
Floating Ground	Black	Left open

The initial and final potentials of -0.5 V and 2 V were applied to the exposed surface of the carbon steel coupon with surface area of 26 cm^2. Also the potential was adjusted to sweep with a scan rate of 0.5 mV s^{-1}. The test was conducted at room temperature (23 ± 1°C). The equivalent weight of A36 carbon steel was 28.25 and the density was 7.85 g cm^{-3}.

4.3 Results and Discussion

4.3.1 XRD Analysis, Phase Composition of the Corrosion Products

The x-ray diffraction technique was conducted on the edge and bottom areas of the crevices (See Fig. 4.1) after the carbon steel coupons were immersed in the test solutions for 60 days at room temperature. Fig. 4.4 shows the x-ray diffraction patterns of the corrosion products formed on the edges of the crevices that had been immersed in the solutions.

It shows that the corrosion products layer formed in all solution concentrations mainly consisted of lepidocrocite (γ-FeOOH) and goethite (α-FeOOH). Lepidocrocite was more abundant in the phase composition of the corrosion products formed in the solution of 10 g l^{-1} H_2SO_4, 1 g l^{-1} NaCl, 3 g l^{-1} $Fe_2(SO_4)_3$. Lepidocrocite is an initial corrosion product that is formed in the primary steps of the iron corrosion; however, it is unstable (Waseda and Suzuki, 2005), and is quickly transformed to goethite, in the presence of oxygen and water, or magnetite (Fe_3O_4) by acting on dissolved iron from the substrate. An adhesive structure and a low free energy of formation make goethite more stable than lepidocrocite (Zise *et al*., 2007).

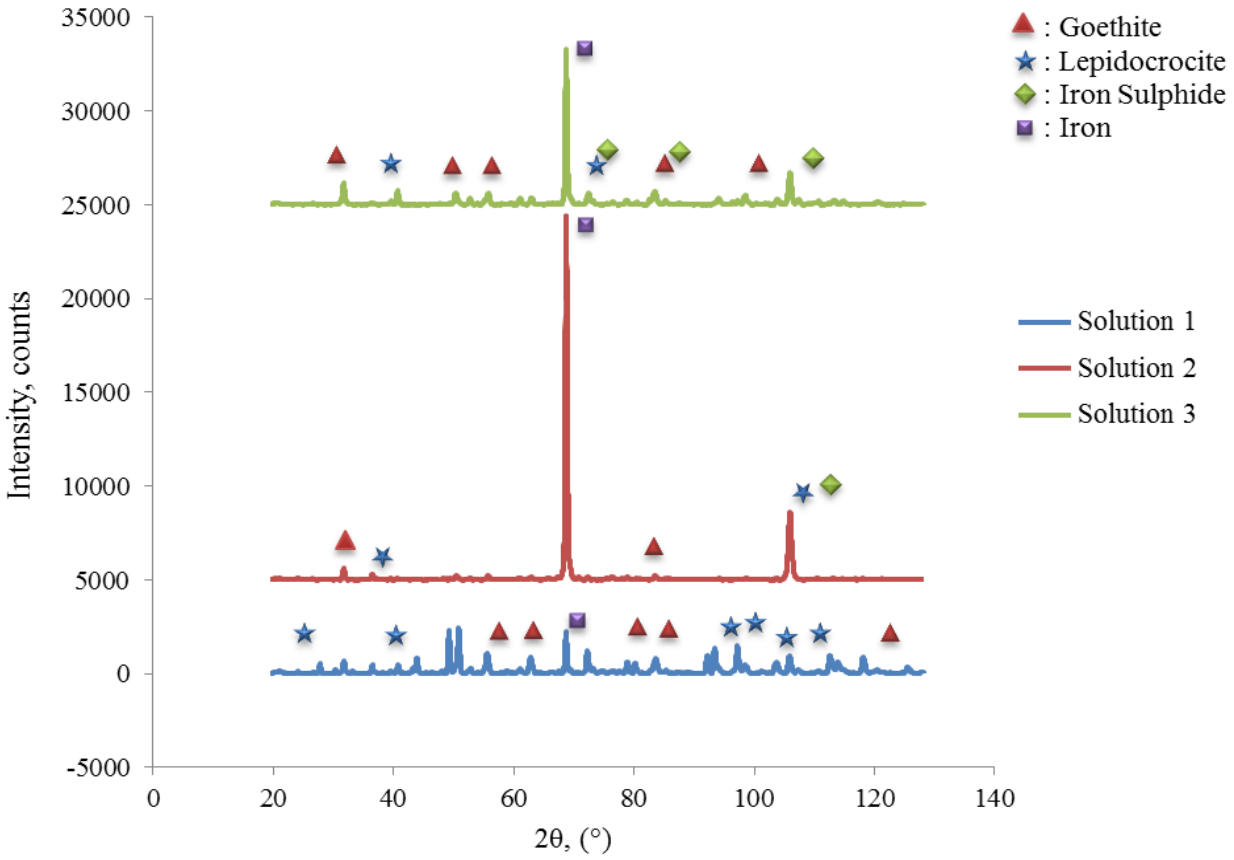

Fig. 4.4. X-ray diffraction patterns of the corrosion products formed on the edges of the crevice after immersion for 60 days at room temperature, Solution 1: 10 g l^{-1} H_2SO_4, 1 g l^{-1} NaCl, 3 g l^{-1} $Fe_2(SO_4)_3$, Solution 2: 50 g l^{-1} H_2SO_4, 1 g l^{-1} NaCl, 3 g l^{-1} $Fe_2(SO_4)_3$, Solution 3: 50 g l^{-1} H_2SO_4, 3 g l^{-1} NaCl, 3 g l^{-1} $Fe_2(SO_4)_3$

In addition to formation of lepidocrocite and goethite, iron and iron (II) sulphide (FeS) spectrums were present in the x-ray diffraction pattern of the corrosion products. The presence of the iron peak indicates that the corrosion products layer was not distributed continuously over the entire surface. Moreover, the iron sulphide was formed at higher concentrations of sulphuric acid. The Pourbaix diagram of carbon steel in sulphuric acid solution at 25°C (Fig. 4.5) shows that iron sulphide is formed in active potentials over a wide range of pH corresponding to reaction (4.1) (Puigdomenech, 2009):

$$8H^{+} + Fe^{2+} + SO_4^{2-} + 8e^{-} \rightarrow FeS\ (c) \qquad (4.1)$$

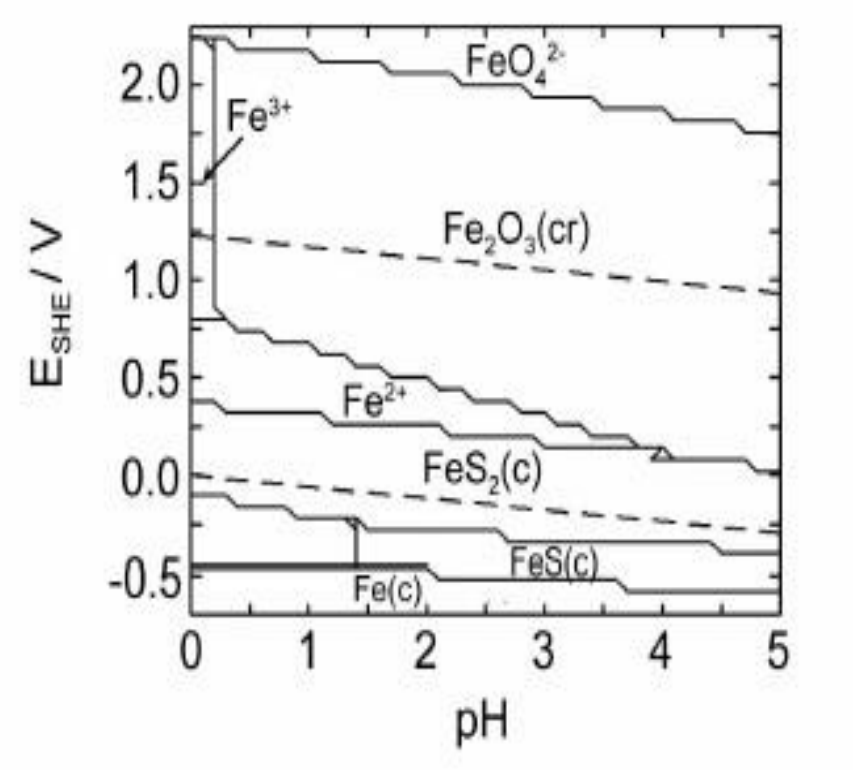

Fig. 4.5. Pourbaix diagram of iron in 0.5 M sulphuric acid solution at 25°C (Tam, 2011)

Lepidocrocite, goethite and magnetite have been identified as the main constituent of the corrosion products formed on carbon steel surfaces exposed to the atmosphere (Antunes *et al*., 2003). However, magnetite was not evident in the XRD pattern of the corrosion products formed on the edges of the coupons with the engineered crevices. Magnetite is an iron oxide consisting of iron (II) and iron (III) ions. The iron (II) ions are in equilibrium with iron, and they are easily oxidized to iron (III) ions. Therefore, magnetite is usually formed in the inner layer of the corrosion products closer to the substrate.

In addition, evidence of akaganeite (β-FeOOH) was not found in the XRD patterns of the corrosion products. Akaganeite is a non-protective corrosion product formed in chloride containing environments. Chloride ions are present in the molecular structure of akaganeite (Cornell and Schwertmann, 2003), and are easily released accelerating iron corrosion. The concentration of chloride ions in the bulk solution influences formation of akaganeite. Therefore, absence of the akaganeite spectrum may correspond to the low concentration of chloride ions in the bulk solution (1 g l^{-1} and 3 g l^{-1} NaCl) and low mass transport of chloride ions into the crevice since the disbonded coating causes the solution remain stagnant within the crevice.

The free energy of formation for different corrosion products are presented in Table 4.2. Magnetite has the lowest free energy of formation among all corrosion products which demonstrates its high thermodynamic stability in the corrosion products layer. On the contrary, the high free energy of formation of akaganeite indicates that it is an unstable corrosion product, and is not an end member of transformations of other iron oxy-hydroxides and iron oxides.

Table 4.2. Free energy of formation for different corrosion products

Corrosion product	Fe_3O_4	Fe_2O_3	α-FeOOH	γ-FeOOH	β-FeOOH
Free Energy of Formation kJ mol^{-1}	-1117.13	-822.16	-495.75	-470.25	-280.74

The x-ray diffraction patterns of the corrosion products, formed on the bottom of the crevices in different solution concentrations, are shown in Fig. 4.6. Hematite and green rust were identified in the phase composition of the corrosion products formed on the bottom areas of the crevices. Green rust is an intermediate corrosion product which is composed of a group of iron oxides consisting of layers of octahedral iron (II) hydroxide in which some iron (II) ions are substituted by iron (III) ions (Cornell and Schwertmann, 2003). It is an unstable corrosion product with various chemical compositions which depend on the environment and the anions present in the solution (Simard *et al*., 2001). It is transformed to goethite or lepidocrocite depending on the solution conditions. The environment conditions influence transformation of iron (II) ions to iron (III) ions. The oxygen may be consumed at a higher rate than it diffuses into the crevice due to occluded condition of the crevice. The depletion of oxygen within the crevice impedes transformation of green rust to a stable corrosion product.

The presence of hematite in the x-ray diffraction patterns of the corrosion products indicates that a diffusion barrier layer was formed on the bottom of the crevice which was not destroyed by attack of the chloride ions. Hematite is a harmless corrosion product which is formed in the outer layers of the corrosion products. It is highly stable and usually the end member of many corrosion products transformations (Cornell and Schwertmann, 2003).

In addition to the formation of green rust and hematite, iron sulphide, iron sulphate and iron spectrums were detected in the phase composition of the corrosion products. Iron sulphate was detected as the concentration of sulphuric acid was increased from 10 g l^{-1} to 50 g l^{-1} (Fig. 4.6). It is formed in concentrated sulphuric acid solutions when dissolved iron (II) reacts with the acid. Moreover, the presence of iron spectrum indicates that the corrosion products layer was not distributed continuously.

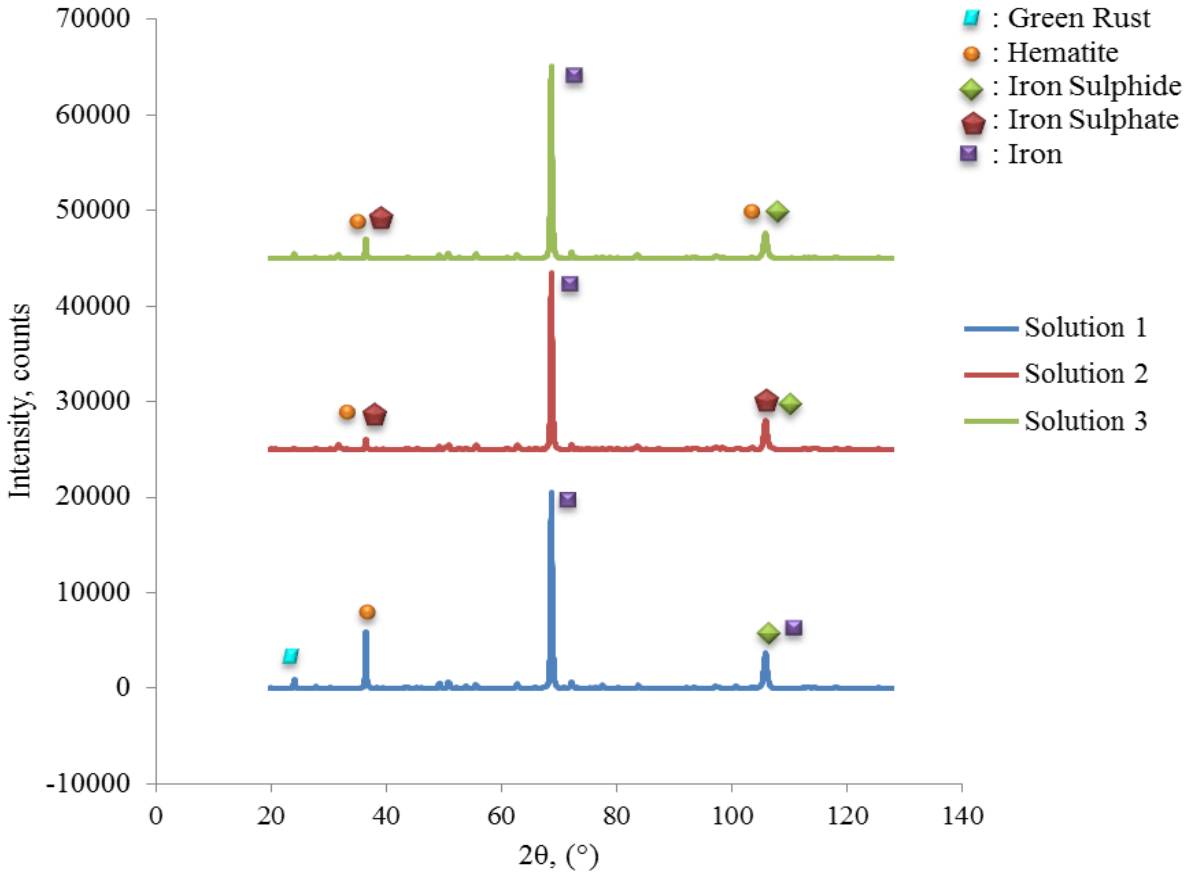

Fig. 4.6. X-ray diffraction patterns of the corrosion products formed on the bottom of the crevices after immersion for 60 days at room temperature, Solution 1: 10 g l^{-1} H_2SO_4, 1 g l^{-1} NaCl, 3 g l^{-1} $Fe_2(SO_4)_3$, Solution 2: 50 g l^{-1} H_2SO_4, 1 g l^{-1} NaCl, 3 g l^{-1} $Fe_2(SO_4)_3$, Solution 3: 50 g l^{-1} H_2SO_4, 3 g l^{-1} NaCl, 3 g l^{-1} $Fe_2(SO_4)_3$

In general, the corrosion products layer has a non-uniform thickness at different areas due to the formation of corrosion products on different layers. Also, there can be reaction of the corrosion products and/or the initial corrosion products react to form iron oxides and/or iron oxy-hydroxides. Consequently, it is difficult to identify all constituents of the corrosion products.

4.3.2 Pitting Corrosion Mechanism and Stages

Based on the results of the SEM and XRD analyses the pitting corrosion of carbon steel with the engineered disbonded coating falls into three stages. Fig. 4.7 shows a schematic diagram of pitting corrosion. In the first stage there is no protective and or non-protective layer on the carbon steel surface. Anodic and cathodic reactions occur simultaneously at different sites of the surface. The anodic dissolution of iron occurs at anode sites due to direct contact of the metal surface and solution as follows:

$$Fe \rightleftharpoons Fe^{2+} + 2e^{-} \quad (4.1)$$

The cathodic reduction of hydrogen ions and oxygen occurs at cathode sites due to the presence of sulphuric acid and oxygen in the solution as follows:

$$O_2 + 4H^{+} + 4e^{-} \rightleftharpoons 2H_2O \quad (4.2)$$

$$1/2O_2 + H_2O + 2e^{-} \rightleftharpoons 2OH^{-} \quad (4.3)$$

In the second stage, the dissolved species from the anodic and cathodic reactions form iron hydroxide that is an initial corrosion product (reaction 4.4). The iron hydroxide is an initial corrosion product that is transformed to iron oxides or iron oxy-hydroxides (reaction 4.5).

$$Fe^{2+} + 2OH^{-} \rightarrow Fe(OH)_2 \quad (4.4)$$

$$Fe(OH)_2 + O_2 \rightarrow Fe_2O_3.H_2O \text{ or } 2FeOOH \quad (4.5)$$

The iron oxides and or iron oxy-hydroxides form the protective layer on the surface that performs as a diffusion barrier. In the third stage, the layer is destroyed by attack of the chloride ions according to reaction (4.6) and (4.7). The iron oxy-hydroxide layer is dissolved to iron (III) ion, and the iron (III) ion performs as an oxidant that accelerates the iron dissolution.

$$FeOOH + Cl^- \rightarrow FeOCl + OH^- \quad (4.6)$$

$$FeOCl + H_2O \rightarrow Fe^{3+} + Cl^- + 2OH^- \quad (4.7)$$

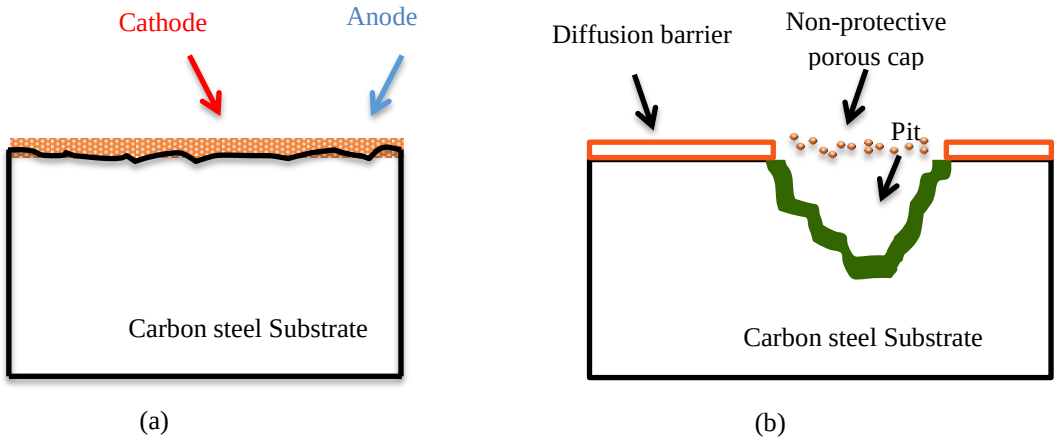

Fig. 4.7. Schematic diagram of pitting corrosion on the carbon steel under the disbonded coating (a) Formation of diffusion barrier, (b) Pitting corrosion initiation

The diffusion barrier disruption causes the direct dissolution of iron into the solution and pitting corrosion initiation. The hydrolysis of the dissolved iron at the disrupted sites causes a decrease in pH and the formation of a differential concentration cell that causes separation of anode/cathode and electron migration. The indirect oxidation of iron (II), due to the presence of chloride ions, causes the formation of a gelatinous cap over the pit mouth as follows:

$$Fe^{2+} + 2H_2O + 2Cl^- \rightarrow Fe(OH)_2 + 2HCl \quad (4.8)$$

4.3.3 Potentiodynamic Measurements

Fig. 4.8 shows the polarization curve of the carbon steel coupon without the crevice. It can be seen that the anodic polarization curve deviates from Tafel behaviour at voltage of -0.47 V which indicated that different major reductants were participating in the anodic reactions. The constituents of the metal cannot participate in the anodic reactions due to the low percentage. Therefore, the deviation from Tafel behaviour in the anodic region was assigned to an active-passive transition or re-oxidization of corrosion products since iron (II) oxides are unstable and tend to be transformed to iron (III) oxides.

The corrosion measurements were accomplished by Tafel extrapolation using the Gamry Echem Analyst^{TM} software (Table 4.3). The measured corrosion current was very small which demonstrated that a diffusion barrier layer was formed on the carbon steel surface. The diffusion barrier layer reduces the rate of mass transfer to the surface thus reducing the oxygen reduction rate with a corresponding drop in corrosion rate.

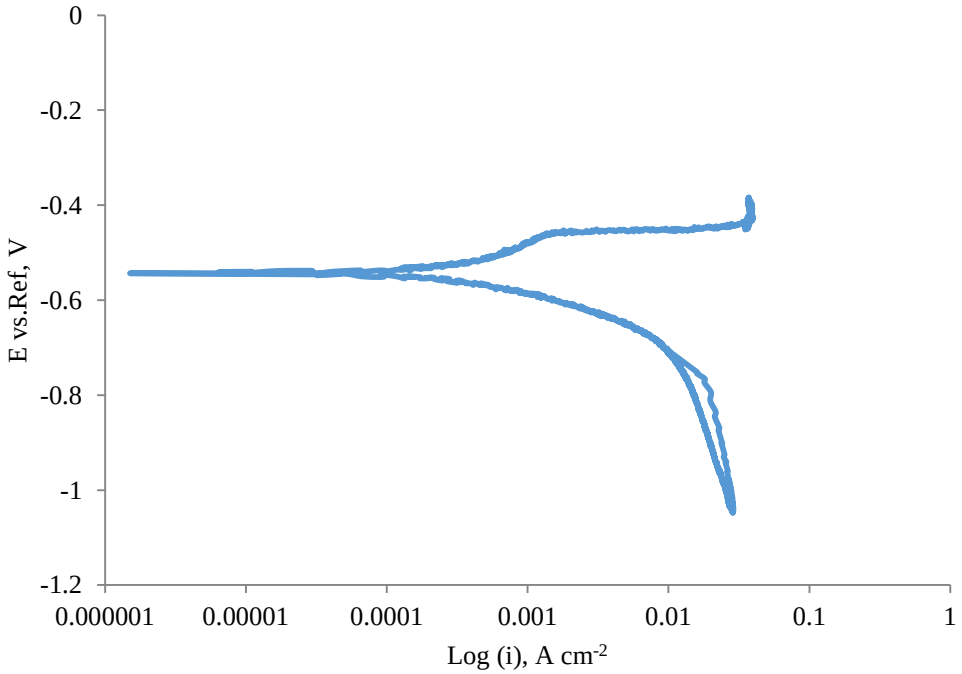

Fig. 4.8. Polarization curve of A36 carbon steel in 50 g l^{-1} of H_2SO_4 containing 3 g l^{-1} of NaCl and 3 g l^{-1} of $Fe_2(SO_4)_3$ at room temperature (23 ± 1°C)

Table 4.3. Corrosion measurements of the potentiodynamic scan for A36 carbon steel immersed in 50 g l^{-1} of H_2SO_4 containing 3 g l^{-1} of NaCl and 3 g l^{-1} of $Fe_2(SO_4)_3$ at room temperature (23 ± 1°C)

β_a	β_c	E_{corr}	E_{ocp}	i_{corr}	Corrosion Rate
V/decade	V/decade	mV	mV	A/cm2	mm/year
1.62E-01	9.48E-02	-543.4	-561.01	3.92E-04	4.61

4.4 Summary and Conclusions

In chapter 4, the phase composition of the corrosion products, the formation of protective and non-protective layers and the corrosion mechanism were investigated by conducting XRD analysis and potentiodynamic test. A36 carbon steel coupons with 1 mm crevice gaps were immersed for 60 days at room temperature to produce a thick scale on the metal surface. XRD

characterization was performed on the edge and bottom of the coupons under the disbonded coating, and the following conclusions were drawn:

1. The corrosion products layer formed on the edge of the carbon steel surface consisted of lepidocrocite and goethite.

2. The corrosion products layer formed on the bottom of the carbon steel surface consisted of hematite and green rust.

3. No akaganeite and magnetite were formed on the edges of the coupons under the disbonded coating.

4. The disruption of diffusion barrier formed on the edges of the coupons caused initiation and propagation of pitting corrosion.

The potentiodynamic scans were conducted on the plain carbon steel coupon that was immersed in the highest solution concentration, and it was concluded that:

1. A small corrosion current passed through the carbon steel electrode. The small corrosion current indicated that a diffusion barrier layer was formed on the surface.

2. The Tafel deviation in the anodic polarization curve corresponded to re-oxidization of the corrosion products.

Chapter Five

5 Corrosion Stages, Current and Potential Changes

5.1 Overview of Chapter 5

Chapter 5 of this thesis covers the last objective of this research project. The electrochemical noise measurement test was conducted in more concentrated solution at room temperature to attempt to identify the corrosion stages occurring under the disbonded coating and measure the current-potential changes within the crevice.

5.2 Experimental Procedure

A three-electrode electrochemical cell was used for the measurements. Two A36 carbon steel coupons were used as working electrodes (WEs), and a saturated calomel electrode (SCE) was used as reference electrode (RE). The carbon steel coupons with exposure areas of 26 cm^2 or 2 cm^2 and crevice gaps of 0.1 mm were used as anode electrodes. The under-surface and sides of the coupons were sealed with epoxy resin. Acrylic coatings with surface areas of 35.75 cm^2 and 3.5 cm^2 were cut from acrylic sheet, and placed on the carbon steel coupons respectively. Teflon™ tapes with thickness of 0.1 mm were placed between the coupons and the coatings to create the engineered crevices. The carbon steel coupons with exposure areas of 26 cm^2 were used as cathode electrodes. The under-surface and sides of the coupons were sealed with epoxy

resin. The exposed surfaces of the coupons were polished with 400 and 600 grit sand paper and rinsed with RO water and acetone. The test solution was 50 g l^{-1} H_2SO_4 containing 3 g l^{-1} NaCl and 3 g l^{-1} $Fe_2(SO_4)_3$. The solution was made of RO water and analytical reagents. The electrodes were immersed in 1 litre of the test solution.

Fig. 5.1 shows the schematic diagram of the WEs and the corrosion cell for ECN measurements. Two carbon steel electrodes, one with the engineered crevice (shown as WE1 in Fig. 5.1; 26 cm^2, 2 cm^2) and another one without the engineered crevice (shown as WE2 in Fig. 5.1; 26 cm^2) were used as the WEs. The area ratio of cathode to anode (r) was 1 and 13. Different area ratios of cathode to anode were chosen to see if this ratio has an effect on crevice corrosion.

The Gamry Interface 1000^{TM} was employed to carry out the electrochemical noise measurements. The potential noise between the coupled WEs and the SCE and the current noise between the two WEs were measured simultaneously using the ZRA mode for the noise measurements. The experiments were conducted continuously for 24 hours at room temperature. A Gamry Faraday Cage was placed over the corrosion cell to enhance quality of the measurements and provide coverage from unwanted environmental noise.

The ECN tests were repeated for type 304 austenitic stainless steel with the same conditions for comparison to the carbon steel case. Crevice corrosion is considered a significant concern when stainless steels are used in chloride containing environments.

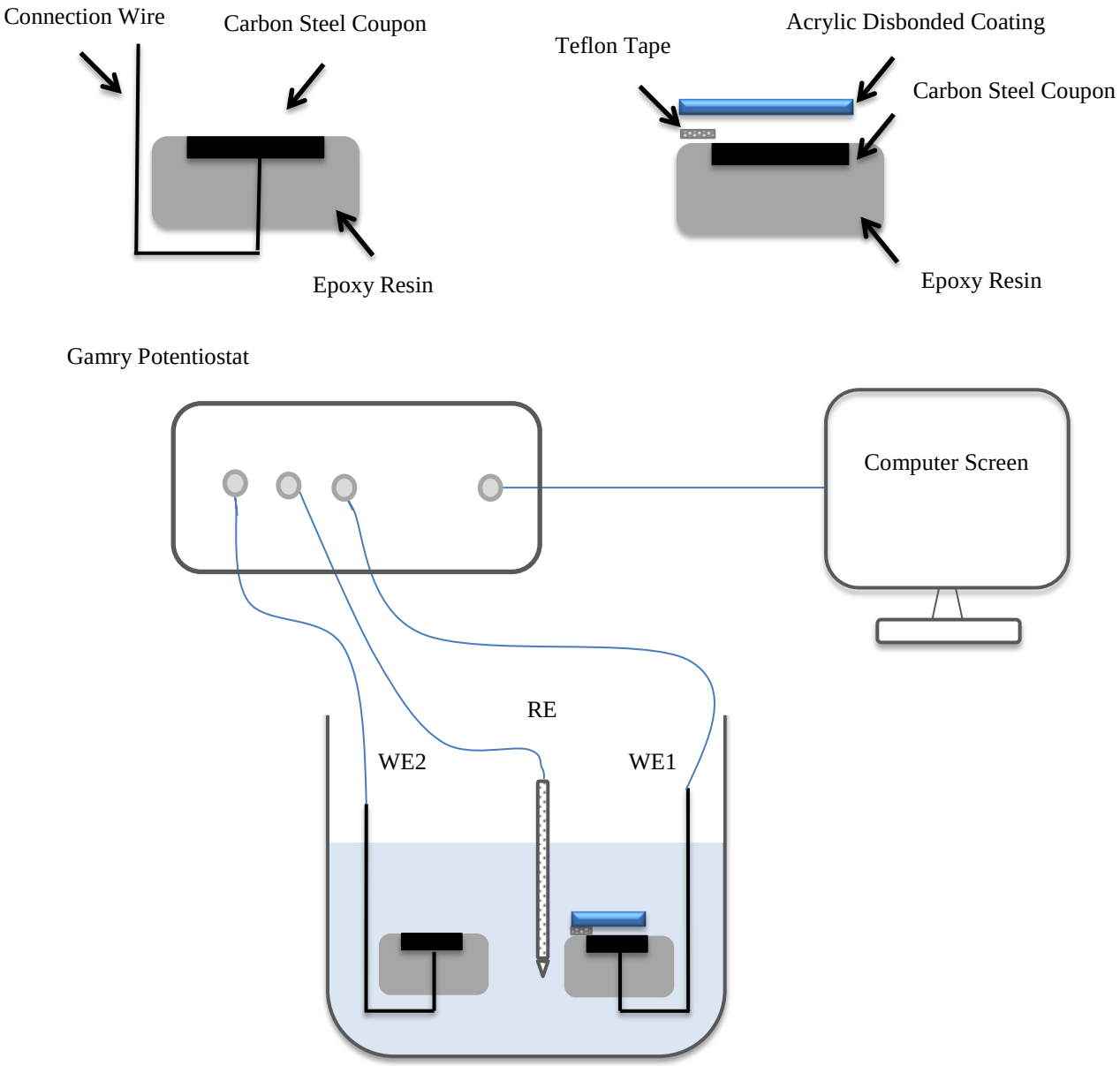

Fig. 5.1. Schematic diagrams of WEs and the corrosion cell for ECN measurements

5.3 Results and Discussion

5.3.1 ECN Measurements for Carbon Steel

Fig. 5.2 shows the current and potential noise measurements over 24 hour for WEs with an area ratio of 1. The potential noise measured between coupled WEs and RE indicates the change in the state of the electrode with the engineered crevice. The current noise measured between the WEs indicates the rate of corrosion within the crevice (Hu *et al.*, 2010). For stainless steel, classical crevice corrosion consists of three stages of incubation, initiation and propagation. During the incubation period a leakage or passive current flows through the film since a protective layer is present on the substrate surface with a poor electrical conductivity. For carbon steel, the passive film does not form on the metal surface. Instead, a diffusion barrier is formed and this may significantly reduce the corrosion rate as is shown in Fig. 5.2 (a).

The potential between the coupled working electrodes and the reference electrode was constant (Fig. 5.2 (b)). The constant potential of the electrodes indicated that the state of the electrodes surface did not change. Also, no transition occurred in the potential noise measurements which showed that the classical crevice corrosion did not occur. The ECN results were inconclusive and it is recommended that this area of the project be investigated further with possibly a different design of the working electrodes.

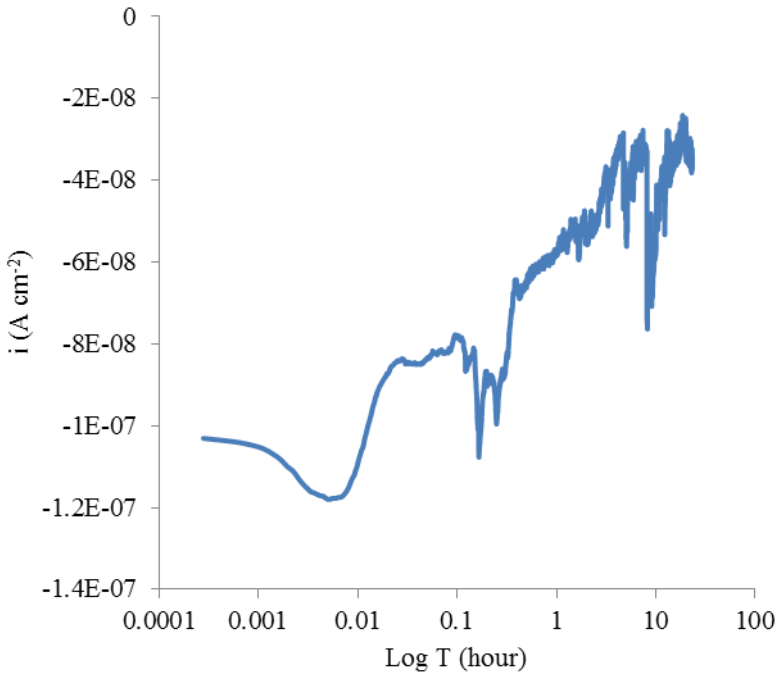

(a)

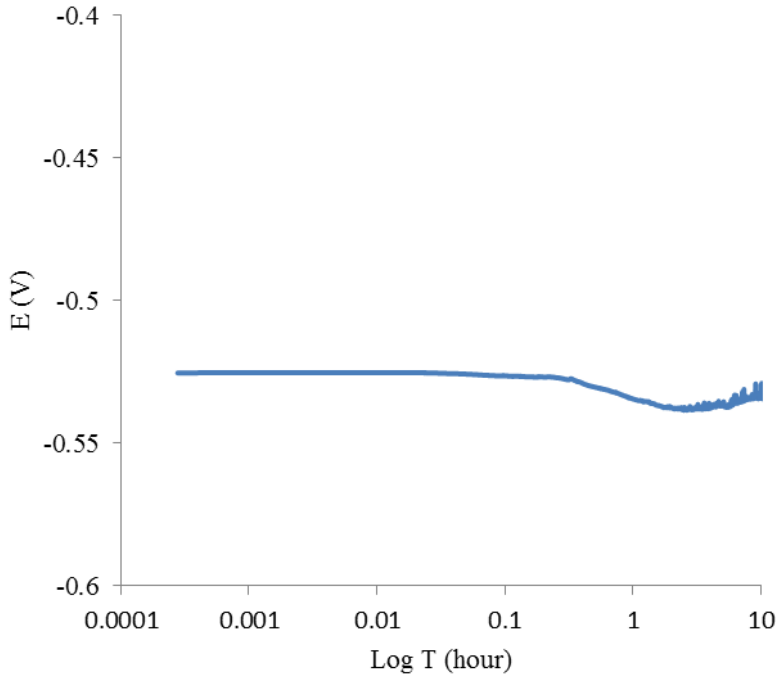

(b)

Fig. 5.2. ECN measurements of A36 carbon steel coupon with crevice gap of 0.1 mm and cathode to anode area ratio of 1 over 24 hour immersed in 50 g l^{-1} H_2SO_4, 3 g l^{-1} NaCl, 3 g l^{-1} $Fe_2(SO_4)_3$, (a) current noise versus time, (b) potential noise versus time

Fig. 5.3 shows the potential and current noise measurements over 24 hour for WEs with area ratio of 13. The current fluctuations occurred in first few hours of the measurements indicated that only general corrosion occurred on the surface of the carbon steel coupons within the crevice. Also, the potential was constant after fluctuations in the first few hours (Fig. 5.3 (b)). The few fluctuations of the potential indicated that the potential difference between the crevice and bold surface (cathode) was small and the crevice corrosion did not develop within the crevice. It can be seen that the potential became more noble as the area ratio of cathode to anode increased.

The frequent current fluctuations for r=1 are assumed to correspond to pit formation. When the absolute current increases, pitting corrosion initiates. It then recovers as repassivation of the pit mouth occurs. If the absolute current does not recover and keeps changing, pit propagation occurs. However, for r=13, the current fluctuations happened during the first few minutes which may correspond to general corrosion and the formation of a diffusion barrier layer. It can be seen that after about 2 hours, the current did not change significantly (see Fig. 5.3 (a)).

The occurrence and development of crevice corrosion is affected by the area ratio of cathode to anode (Hu *et al*., 2010). As the area ratio of cathode to anode increases the corrosion rate and current flowing from anode to cathode increase. However, in this case the current was greater and the potential was more active as the area ratio of cathode to anode decreased. This might be due to the chemical composition of the solution including the presence of oxidizing agents.

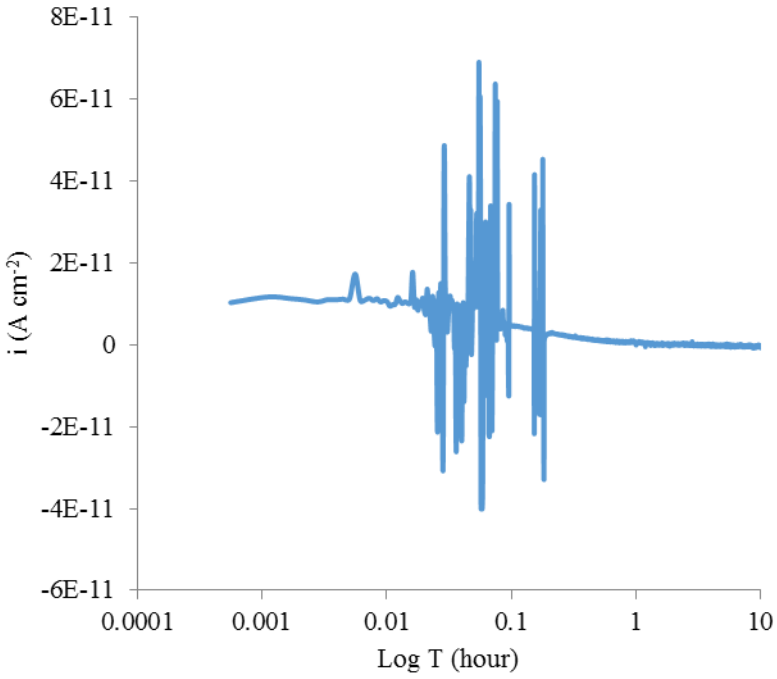

(a)

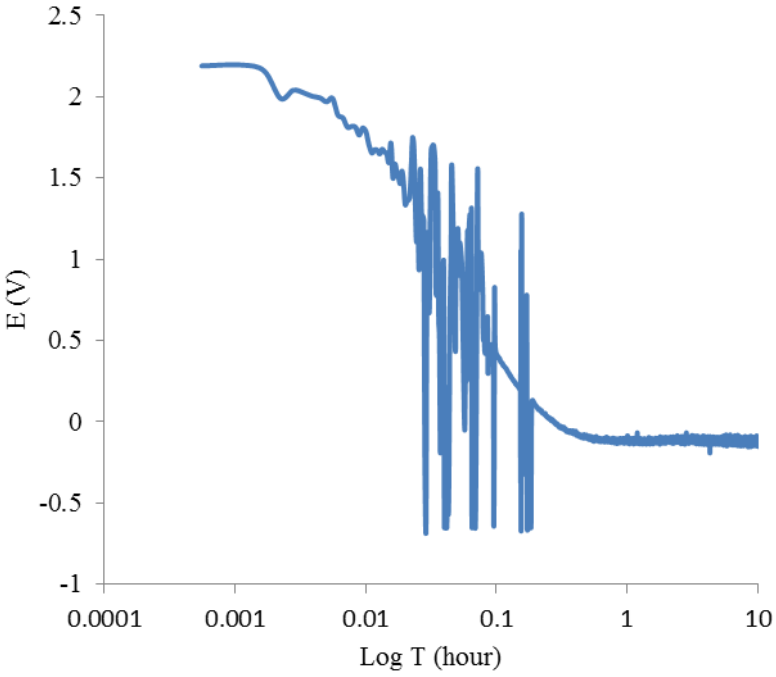

(b)

Fig. 5.3. ECN measurements of A36 carbon steel coupon with crevice gap of 0.1 mm and cathode to anode area ratio of 13 over 24 hour immersed in 50 g l^{-1} H_2SO_4, 3 g l^{-1} NaCl, 3 g l^{-1} $Fe_2(SO_4)_3$, (a) current noise versus time, (b) potential noise versus time

5.3.2 ECN Measurements for Stainless Steel

The results of the ECN measurements for 304 stainless steel coupons with area ratio of 1 are presented in Fig. 5.4. The current fluctuations lasted for approximately 2 hours, and then remained relatively constant. The potential was constant after a negative shift in the first few hours of the measurements. When the potential shifted negatively at hour 2, the current increased simultaneously. The constant current and potential after 2 hours indicates that the corrosion entered to the stable state.

Fig. 5.5 shows the results of the ECN measurements for 304 stainless steel coupons with area ratio of 13. The frequent current fluctuations were seen for area ratio of 13 over 24 hours. As the area ratio increased from 1 to 13, the potential was more active and the current was more accelerated.

According to the ECN measurements for 304 stainless steel coupons, significant potential fluctuations were seen for the 304 stainless steel coupons unlike carbon steel, which showed a relative stable potential. This indicates that damage to the passive film on the stainless steel might have been occurring, which could in turn have been due to the onset of crevice corrosion. However, since the current densities in both cases were small, any damage to the surfaces would have been correspondingly small.

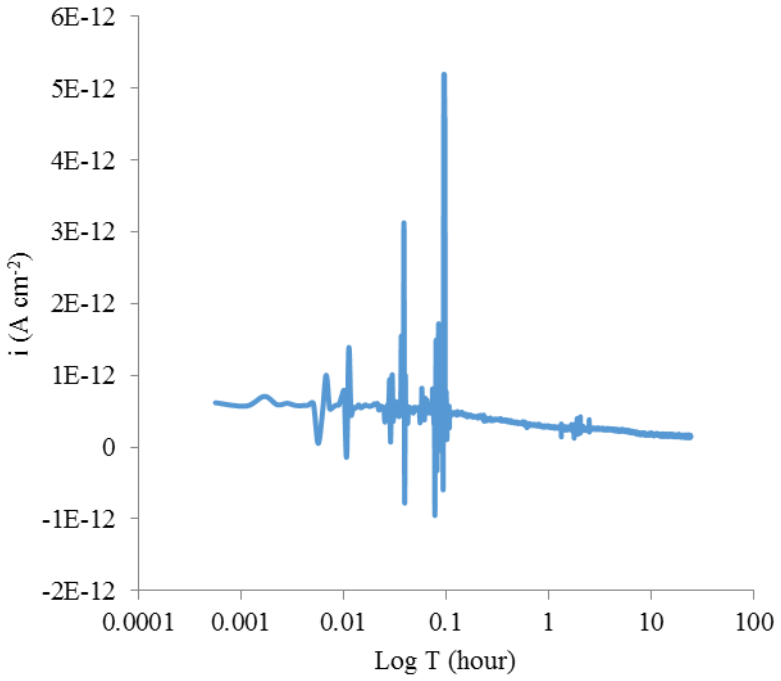

(a)

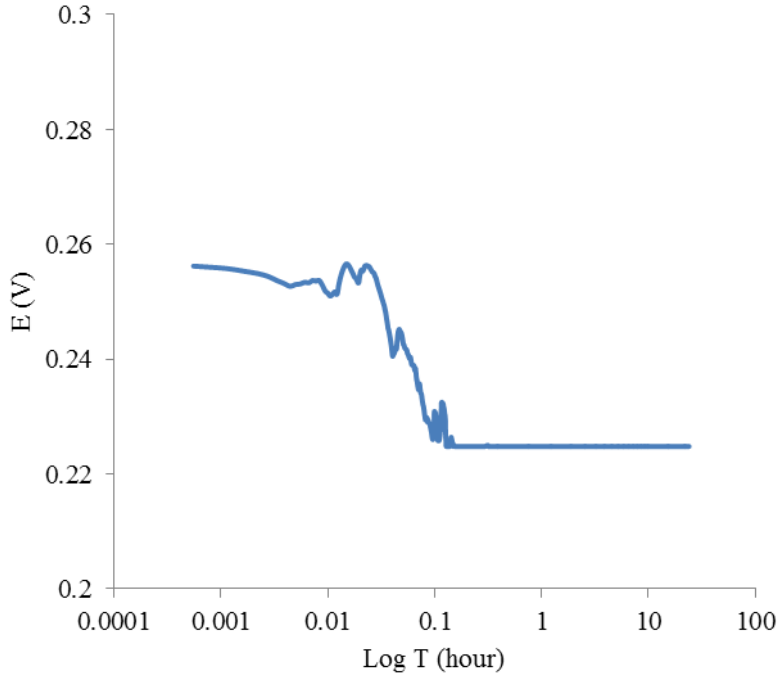

(b)

Fig. 5.4. ECN measurements of 304 Stainless steel coupon with crevice gap of 0.1 mm and cathode to anode area ratio of 1 over 24 hour immersed in 50 g l^{-1} H_2SO_4, 3 g l^{-1} NaCl, 3 g l^{-1} $Fe_2(SO_4)_3$, (a) current noise versus time, (b) potential noise versus time

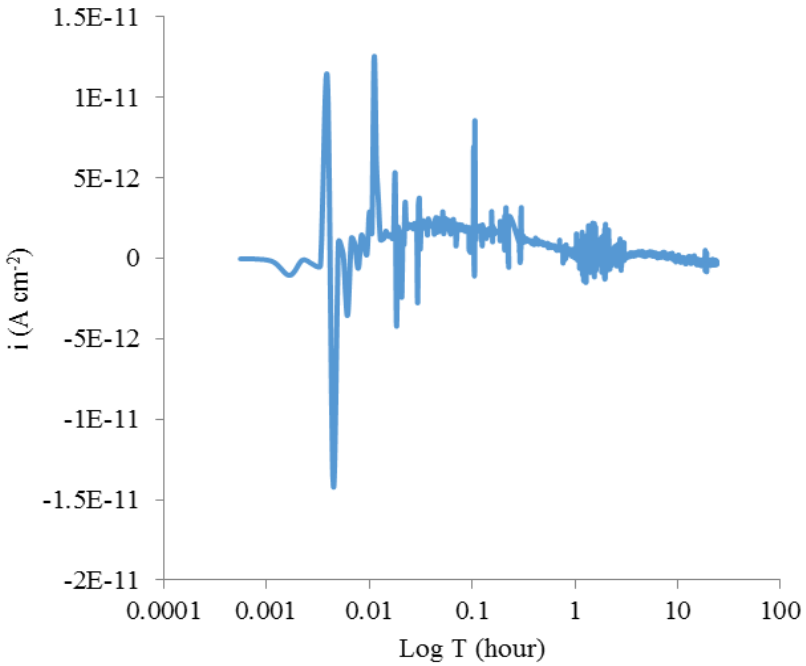

(a)

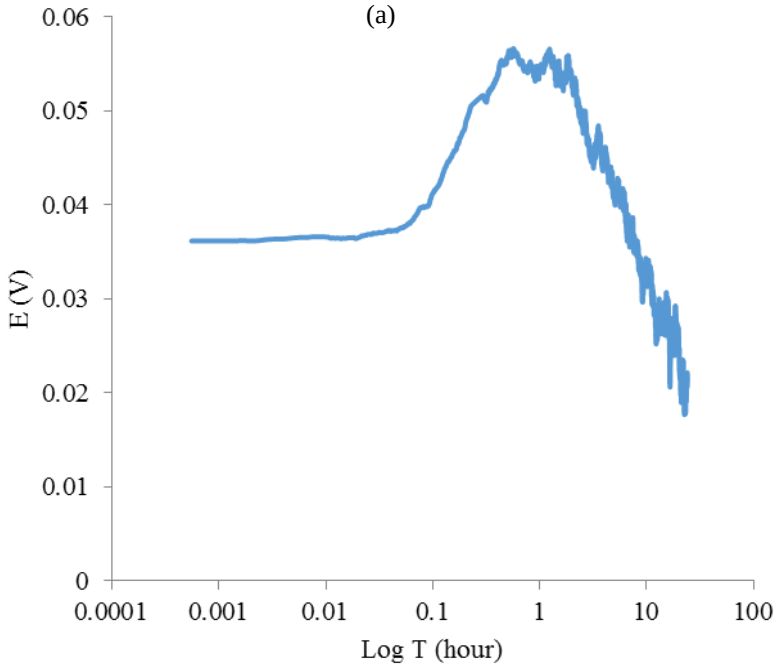

(b)

Fig. 5.5. ECN measurements of 304 Stainless steel coupon with crevice gap of 0.1 mm and cathode to anode area ratio of 13 over 24 hour immersed in 50 g l^{-1} H_2SO_4, 3 g l^{-1} NaCl, 3 g l^{-1} $Fe_2(SO_4)_3$, (a) current noise versus time, (b) potential noise versus time

5.4 Summary and Conclusions

The ECN measurements were conducted for the system of two WEs and one RE. The first WE was a plane carbon steel coupon without the crevice, and the other had the engineered crevice with thickness of 0.1 mm. Two different area ratios of cathode to anode were tested and it was concluded that:

1. Classical crevice corrosion which consists of incubation, initiation and propagation stages, did not initiate for different area ratios of cathode to anode.

2. The smaller area ratio of cathode to anode caused the more active potential and the greater current.

The ECN measurements were repeated for 304 stainless steel coupons with the same conditions used for A36 carbon steel coupons, and it was concluded that the state of the crevice was changed and the crevice corrosion initiated. However, the corrosion was not accelerated due to the low current passing through the crevice electrode.

Chapter Six

6 Summary, Conclusions and Recommendations

6.1 Summary and Conclusions

This thesis focuses on the corrosion behaviour of A36 carbon steel with the engineered disbonded coating in acidified leaching circuits containing sodium chloride and iron (III) sulphate. This thesis described the experimental work and the results of the tests performed to complete the research project objectives. SEM and XRD analyses were conducted to investigate the morphology and phase composition of the corrosion products formed on the carbon steel surface (Chapter 3 and 4). Acrylic spacers were used to create the engineered crevices and disbonded coatings respectively. The immersion test was performed in several solution concentrations at 55 ± 0.1°C for 14 days. The SEM analysis of the carbon steel surfaces showed that pitting corrosion and general corrosion occurred in all solution concentrations. Moreover, the structure of the corrosion products was compact and continuous outside the pits providing a good protection against diffusion of corrosion species and further corrosion.

The carbon steel coupons were immersed in the same solution concentrations with different test conditions to obtain a thick layer of the corrosion products for XRD analysis. The immersion test was performed at room temperature (23 ± 1°C) for 60 days. The XRD analysis of

the corrosion products formed on the surface of the coupons indicated that the corrosion products were different on different areas of the crevice. Lepidocrocite and goethite were the main constituents of the corrosion products formed on the sides of the crevice while green rust and hematite were the main constituents of the corrosion products formed on the bottom of the crevice.

The current-potential changes and the corrosion process within the crevice were studied by electrochemical noise measurements (Chapter 5). A system of two WEs and one RE was used for the noise measurements. The first WE had the engineered crevice, and the second one was a plain carbon steel coupon without the engineered crevice. Teflon^{TM} tapes were used to create the engineered crevices and placed between the carbon steel coupons and the acrylic coatings. Current and potential noise measurements taken over a 24 hour period showed that the crevice corrosion did not occur on the carbon steel surface. This may corresponded to the solution concentration and or the crevice geometry. Furthermore, frequent fluctuations of the current and the constant potential indicated that only general and pitting corrosion occurred on the carbon steel surface within the crevice.

6.2 Future Work and Recommendations

Some topics are recommended for the future work to verify the results of the experiments and study the corrosion of carbon steel under the disbonded coating in sulphuric acid solutions containing chloride ions. These topics are as follows:

1. The crevice geometry, solution concentration and pH influence the occurrence, stages and rate of the crevice corrosion. In this research project, the crevice corrosion did not occur on the carbon steel surface in acidified chloride solutions. The concentration of

sodium chloride in the leach solution was very low. Moreover, there is no study on the corrosion of carbon steel in acidic solutions containing chloride ions. Therefore, the crevice geometry and the sodium chloride concentration can be changed to investigate crevice corrosion in these conditions.

2. A system of two WEs and one RE was used for the ECN measurements of the carbon steel coupons, and crevice corrosion was not observed. A different design of the WEs can be used to investigate occurrence of the crevice corrosion.
3. The crevice thickness for the immersion tests can be reduced to create a tight crevice so that the solution remains stagnant within the crevice, and oxygen diffuses into the crevice at a slower rate.

References

Antunes, R.A., Costa, I., Faria, D.L., 2003. Characterization of corrosion products formed on steels in the first months of atmospheric exposure, J. Material Research, **6(3)**, 403-408.

Betts, A.J., Boulton, L.H., 1993. Crevice corrosion: mechanism, modeling and mitigation, J. B. Corr., **28**, C256-C268.

Bragadireanu, M., Popa, N., Filip, D., Nica, L., 2002. Comparative procedures for uranium solubilization from ores using the leaching method, IAEA, Beijing, 254-261.

Caceres, L., Vargas, T., Herrera, L., 2009. Influence of pitting and iron oxide formation during corrosion of carbon steel in unbuffered NaCl solutions, J. Corrosion Science, **51**, 971-978.

Cornell, R.M., Schwertmann, U., 2003. The iron oxides: structure, properties, reactions, occurrences and uses, 2nd ed, Weinheim, Germany.

Etor, A., 2009. Electrochemical measurement of crevice corrosion of type AISI 304 stainless steel, MSc. Thesis, Department of Chemical Engineering, University of Saskatchewan, SK, Canada.

Evitts, R.W., 1997. Modelling of crevice corrosion, PhD. Thesis, Department of Chemical Engineering, University of Saskatchewan, SK, Canada.

Gamry interface 1000™ potentiostat/galvanostat operator's manual, 2012. Gamry Instruments.

Ghahremaninezhad A., Wang W., 2012. Electrochemical and corrosion behavior of stainless steels 316L and 317L in chloridised ammonium sulphate solution, Canadian Metallurgical Quarterly, **51(4)**, 471-484.

Henley, E.J., 1981. Equilibrium-stage separation operations in chemical engineering, Wiley, New York.

Heppner, K.L., Evitts, R.W., Postlethwaite, 2004. Effect of the crevice gap on the initiation of crevice corrosion in passive metals, J. Corrosion, **60(8)**, 718-728.

Heppner, K.L., 2006. Development of predictive models of flow induced and localized corrosion, PhD. Thesis, Department of Chemical Engineering, University of Saskatchewan, SK, Canada.

Hu, Q., Qiu, Y.B., Guo, X.P., Huang, J.Y., 2010. Crevice corrosion of Q235 carbon steels in a solution of NaHCO3 and NaCl, J. Corrosion Science, **52**, 1205-1212.

Jones, D.A., 1996. Principles and prevention of corrosion, 2nd ed, Prentice-Hall, Upper Saddle River.

Kawashima, A., Yu, W.P., Zhang, B.P., Habazaki, H., Asami, K., Hashimoto, K., 1997. Pitting corrosion of amorphous Ni-Zr alloys in chloride ion containing sulphuric acid solutions, J. Materials Transactions, **38(5)**, 443-450.

Kennell, G.F., Evitts, R.W., 2009. Crevice corrosion cathodic reactions and crevice scaling laws, J. Electrochimica Acta, **54**, 4696-4703.

Kennell G.F., Evitts R.W., Heppner K.L., 2008. A critical crevice solution and IR drop crevice corrosion model, J. Corrosion Science, **50**, 1716-1725.

Loto C.A., 2012. Electrochemical noise measurement technique in corrosion research, J. Electrochemical Science, **7**, 9248-9270.

Loto, R.T., 2013. Pitting corrosion evaluation of austenitic stainless steel type 304 in acid chloride media, J. Mater. Environ. Sci., **4(4)**, 448-459.

Malik, A.U., Prakash, T.L., Ahmad, S., Andijani, I.N., Al-Muaili, F., Jamaluddin, T.M., 2001. Crevice corrosion of high alloy stainless steel in swro pilot plant, Saline water conversion corporation, Saudi Arabia.

Marcus P., 2002. Corrosion mechanism in theory and practice, 2nd ed, New York.

Miki, H., Nicol, M., 2009. The kinetics of the oxidation of iron (II) by chlorate in the leaching of uranium ores, J. Hydrometallurgy, **100**, 47-49.

Oldfield J.W., Sutton, W.H., 1978. Crevice corrosion of stainless steels, II. experimental studies, J. Br. Corros., **13**, 104.

Oldfield J.W., Sutton, W.H., 1978. Crevice corrosion of stainless steels, I. a mathematical model, J. Br. Corros., **13**, 13.

Panossian, Z., Almeida, N.L., Sousa, R.M., Pimenta, G.S., Marques, L.B., 2012. Corrosion of carbon steel pipes and tanks by concentrated sulphuric acid: a review, J. Corrosion Science, **58**, 1-11.

Perdomo, J.J., Singh, P.M., 2002. Electrochemical noise (ECN) measurements as a corrosion monitoring tool: a review, Corrosion Reviews, **20**, 359-378.

Puigdomenech, I., 2009. Make equilibrium diagrams using sophisticated algorithms (MEDUSA), Royal Institute of Technology, Stockholm, Sweden.

Schweitzer, PA., 2007. Corrosion of linings & coatings: cathodic and inhibitor protection and corrosion monitoring, 2nd ed.

Seidel D.C., 1981. Extracting uranium from its ores, International Atomic Energy Agency, Vienna, Austria. Div. of Nuclear Fuel Cycle, **23(2)**.

Simard, S., Odziemkowski, M., Irish, D.E., Brossard, L., Menard, H., 2001. In situ micro-Raman spectroscopy to investigate pitting corrosion product of 1024 mild steel in phosphate and bicarbonate solutions containing chloride and sulphate ions, J. Applied Electrochemistry, **31(8)**, 913-920.

Takahashi, Y., Matsubara, E., Suzuki, S., Okamoto, Y., 2005. In-situ x-ray diffraction of corrosion products formed on iron surfaces, J. Materials Transactions, **46(3)**, 637-642.

Tam, P.L., 2011. Tailoring of transition metal silicides as protective thin films on austenitic stainless steel, PhD. Thesis, Sweden.

Uranium processing, 2008, International Mining, 58-61.

Venter, R., and Boylett, M., 2009. The evaluation of various oxidants used in acid leaching of uranium, Hydrometallurgy Conference, Southern Africa, 445-456.

Wang, H., 2005. Application of electrochemical noise technique in multiphase flow, NACE International Corrosion Conference.

Wang, W., Wang, Q., Wang, C., Yi, J., 2014. Experimental studies of crevice corrosion for buried pipeline with disbonded coatings under cathodic protection, J. Loss Prevention in the Process Industries, **29**, 163-169.

Waseda, Y., Suzuki, S., 2005. Characterization of corrosion products on steel surface, Springer, Tokyo, Japan.

Wolfe, R.C., Weil, K.G., Pickering, H.W., 2004. Electrochemical probes for metal/electrolyte system characterization during crevice corrosion, J. Phys. Chem., **108**, 14298-14304.

Yan, M.C., Wang, J.Q., Han, E.H., Ke, W., 2007. Electrochemical measurements using combination microelectrode in crevice simulating disbonded of pipeline coatings under cathodic protection, J. Corrosion Engineering, **42(1)**, 42-49.

Yousif, E.H., 2006. Extraction and purification of yellow cake, B.Sc. Thesis, Department of Chemistry, Sudan Academy of Science.

Zho, J.M., Zuo, Y., 2007. Corrosion behaviour in simulated solutions within pits and crevices on carbon steel, J. Corrosion Engineering, **42(3)**, 203-206.

Zise, W., Chunchun, X., Xia, C., Ben, X., 2007. The Morphology, phase composition and effect of corrosion products on simulated archaeological, J. Chem. Eng., **15**, 433-438.

Appendix A

A EDS Analysis of the Corrosion Products

This appendix includes the results of EDS (Energy Dispersive X-ray Spectroscopy) analysis. The EDS analysis of the carbon steel coupons was conducted after the immersion test in order to identify the elemental composition of the corrosion products.

A.1 Experimental Procedure

A carbon steel coupon with an engineered crevice with thickness of 1 mm was immersed in a solution of 50 g l^{-1} H_2SO_4 containing 3 g l^{-1} NaCl and 3 g l^{-1} $Fe_2(SO_4)_3$ for 14 days at 55±0.1°C. The Hitachi SU6600 field emission gun scanning electron microscope was employed to carry out the EDS analysis on the carbon steel surface. The EDS analysis was conducted over the entire scan area of the SEM with accelerating voltage of 20 kV.

A.2 Results and Discussion

Fig. A.1 shows the EDS spectrum of the corrosion products formed on the carbon steel surface. The EDS spectrum of the corrosion products indicated that iron and oxygen were clearly the main constituents of the elements. In addition to presence of the iron and oxygen spectrums, Cu, Cr, S, Ni and Si spectrums with low proportion were identified that can be assigned to contaminants and alloy composition.

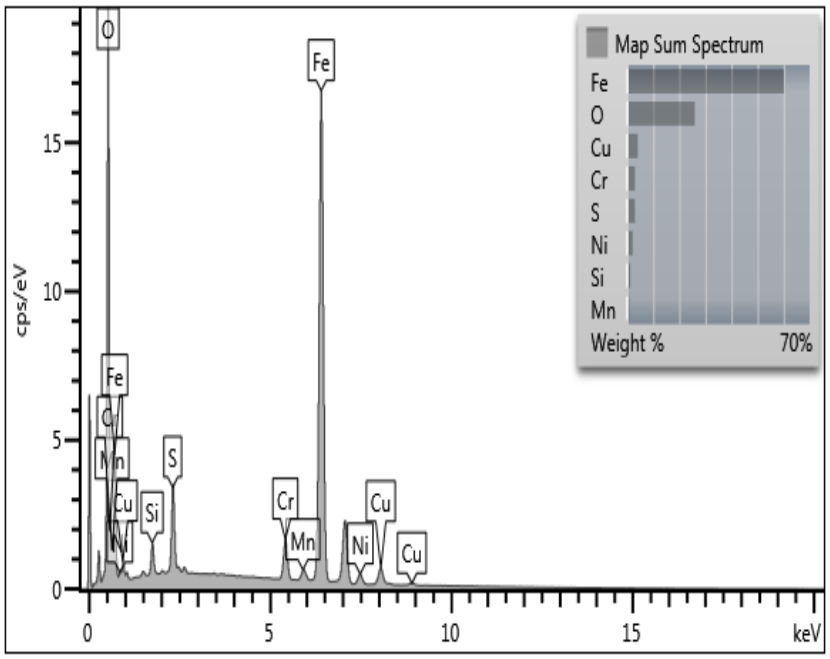

Fig. A.1. EDS spectrum of A36 carbon steel surface immersed in 50 g l^{-1} of H_2SO_4 containing 3 g l^{-1} NaCl and 3 g l^{-1} $Fe_2(SO_4)_3$ for 14 days at 55±0.1°C

A distribution map and relative intensity of the elements, which were identified in the EDS spectrum of the surface, is shown in Fig. A.2. The element map of the corrosion products showed that iron and oxygen covered the most parts of the carbon steel surface. Bright points and regions in the map represented formation of iron sulphide compounds.

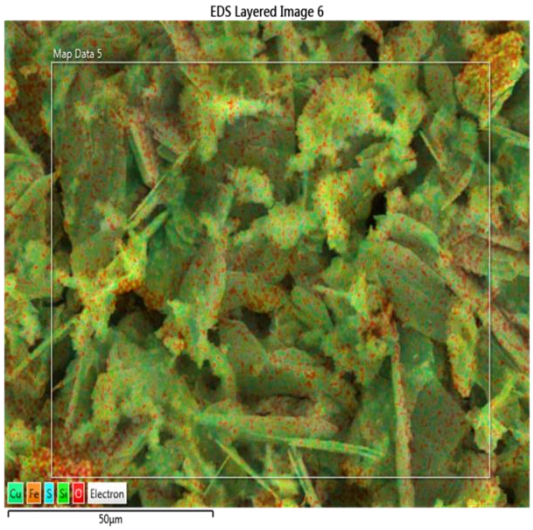

(a)

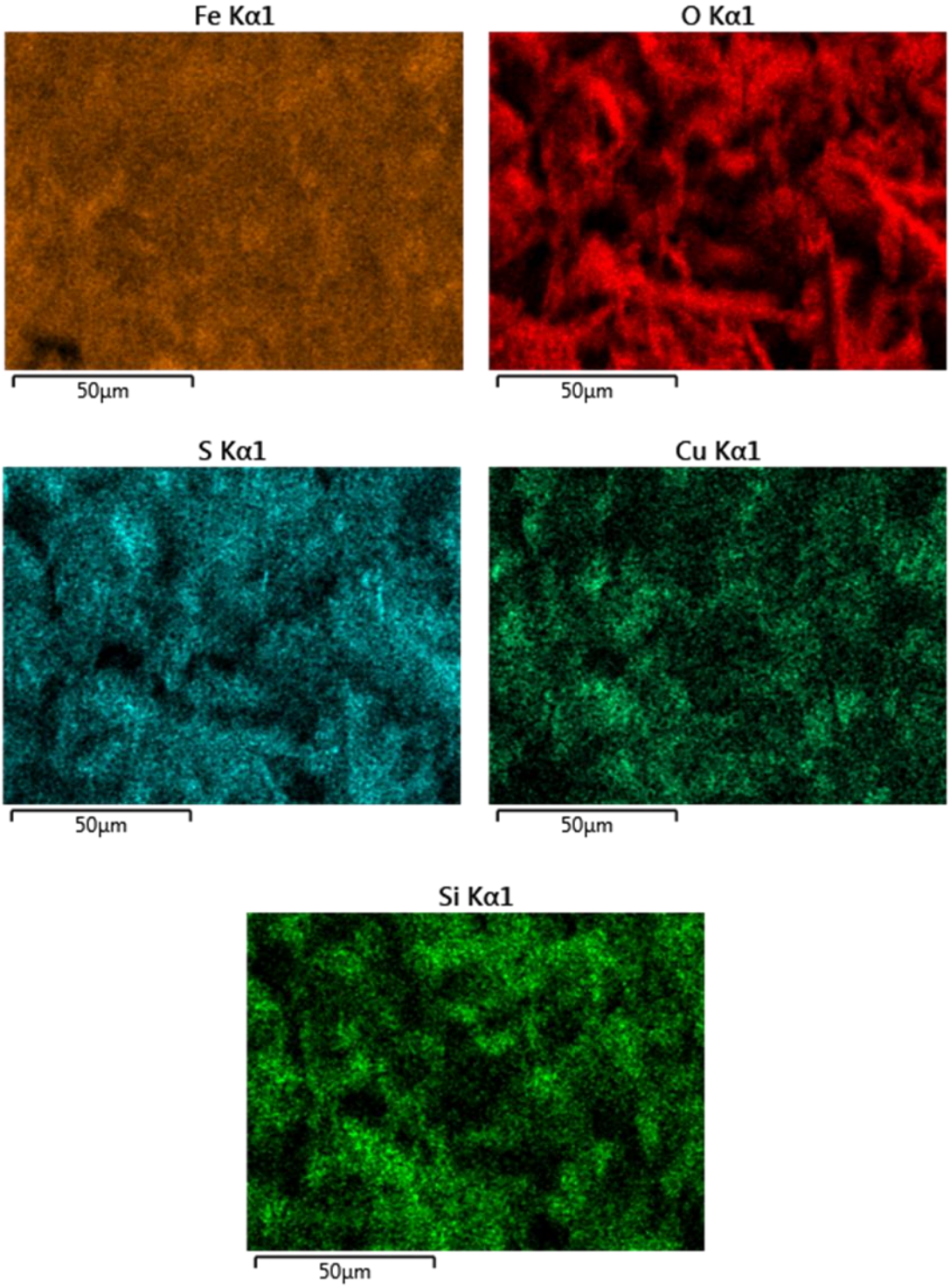

(b)

Fig. A.2. Element map of the corrosion products formed on the carbon steel surface after immersion in 50 g l^{-1} of H_2SO_4 containing 3 g l^{-1} NaCl and 3 g l^{-1} $Fe_2(SO_4)_3$ for 14 days at 55±0.1°C, (a) EDS over the entire scan area of the SEM (b) Elements distribution

Appendix B

B XRD Analysis of the Corrosion Products

This appendix includes the XRD analysis results for sulphuric acid solutions containing sodium chloride. The XRD analysis of the carbon steel coupons was conducted after the immersion test in order to examine the corrosion products phase composition in absence of iron (III) sulphate.

B.1 Experimental Procedure

The carbon steel coupons with the engineered crevices with thickness of 1 mm where immersed in different solution concentrations for 60 days at room temperature. Table B.1 shows concentrations of chemicals in different solutions. The x-ray diffraction technique was conducted on the edge and bottom areas of the crevice after the carbon steel coupons were immersed in the test solutions for 60 days at room temperature.

Table B.1. Chemicals concentrations in different solutions

Chemicals / Conc. ($g\ l^{-1}$)	Solution 1	Solution 2	Solution 3
H_2SO_4	10	10	50
NaCl	1	3	1
$Fe_2(SO_4)_3$	0	0	0

B.2 Results and Discussion

Fig. B.1 represents the x-ray diffraction pattern of the corrosion products formed on the edges of the crevices in different solution concentrations. Lepidocrocite, goethite and hematite

were the main constituents of the corrosion products. Therefore, hematite was added to the phase composition of the corrosion products in absence of iron (III) sulphate.

Several lepidocrocite spectrums were identified in the phase composition of the corrosion products formed in the solutions of 10 g l^{-1} H_2SO_4. The number of the lepidocrocite peaks decreased as the concentration of sulphuric acid increased from 10 g l^{-1} to 50 g l^{-1}. Moreover, hematite spectrums were identified in the phase composition of the corrosion products which demonstrated formation of a very protective diffusion barrier. However, the intensity of the hematite spectrums was low.

Fig. B.2 represents the x-ray diffraction pattern of the corrosion products formed on the bottom of the crevices in different solution concentrations. Green rust and hematite were identified as the main constituents of the corrosion products in presence and absence of the iron (III) sulphate. Therefore, the iron (III) sulphate did not affect the formation of various corrosion products on the bottom of the crevices. Also, the iron sulphate spectrum was identified as the concentration of sulphuric acid increased from 10 g l^{-1} to 50 g l^{-1}. It is formed in high sulphuric acid solutions with the reaction of dissolved iron (II) ions and sulphuric acid.

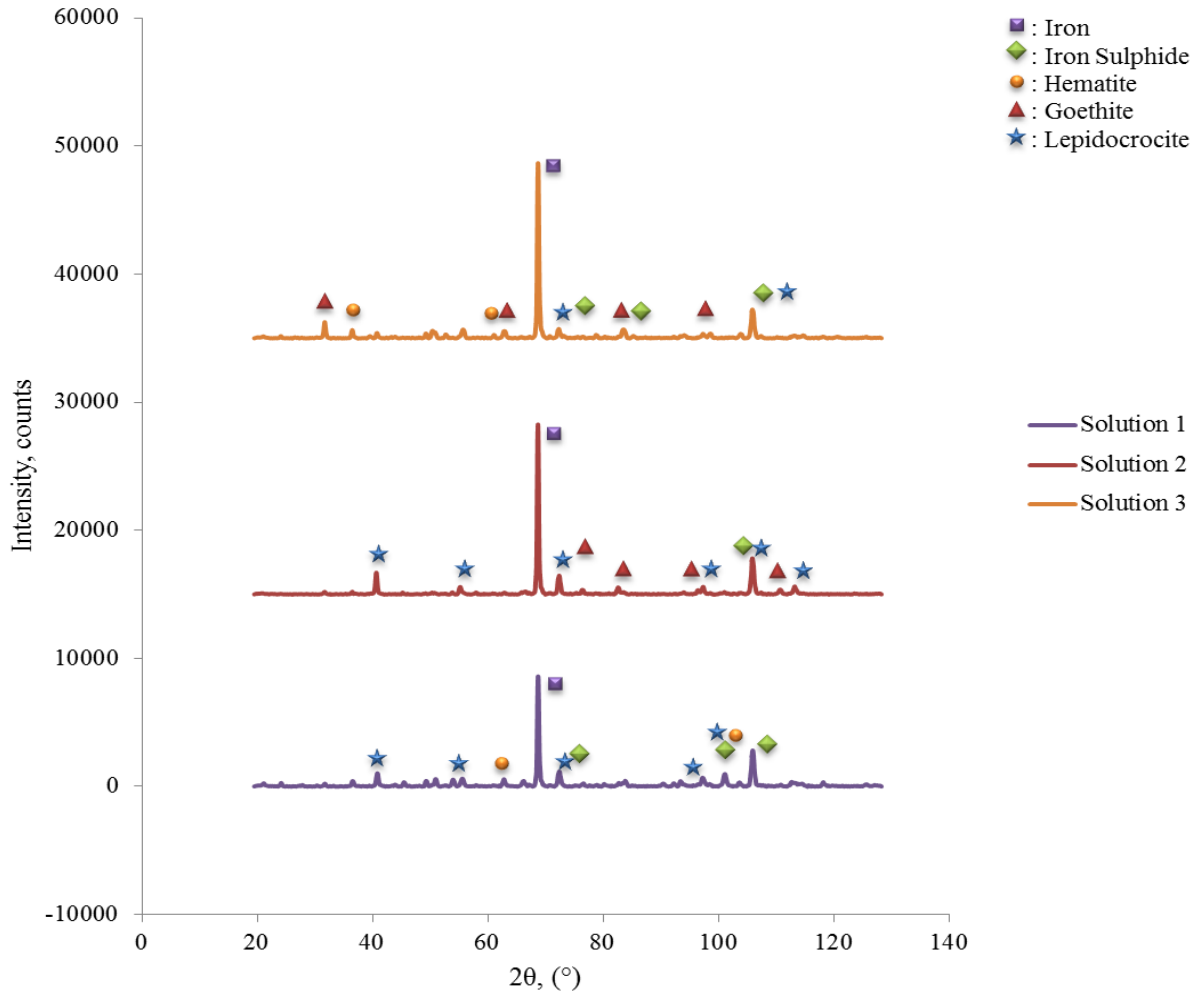

Fig. B.1. X-ray diffraction pattern of the corrosion products formed on the edges of the crevice after immersion for 60 days at room temperature, Solution 1: 10 g l^{-1} H_2SO_4, 1 g l^{-1} NaCl, Solution 2: 10 g l^{-1} H_2SO_4, 3 g l^{-1} NaCl, Solution 3: 50 g l^{-1} H_2SO_4, 1 g l^{-1} NaCl

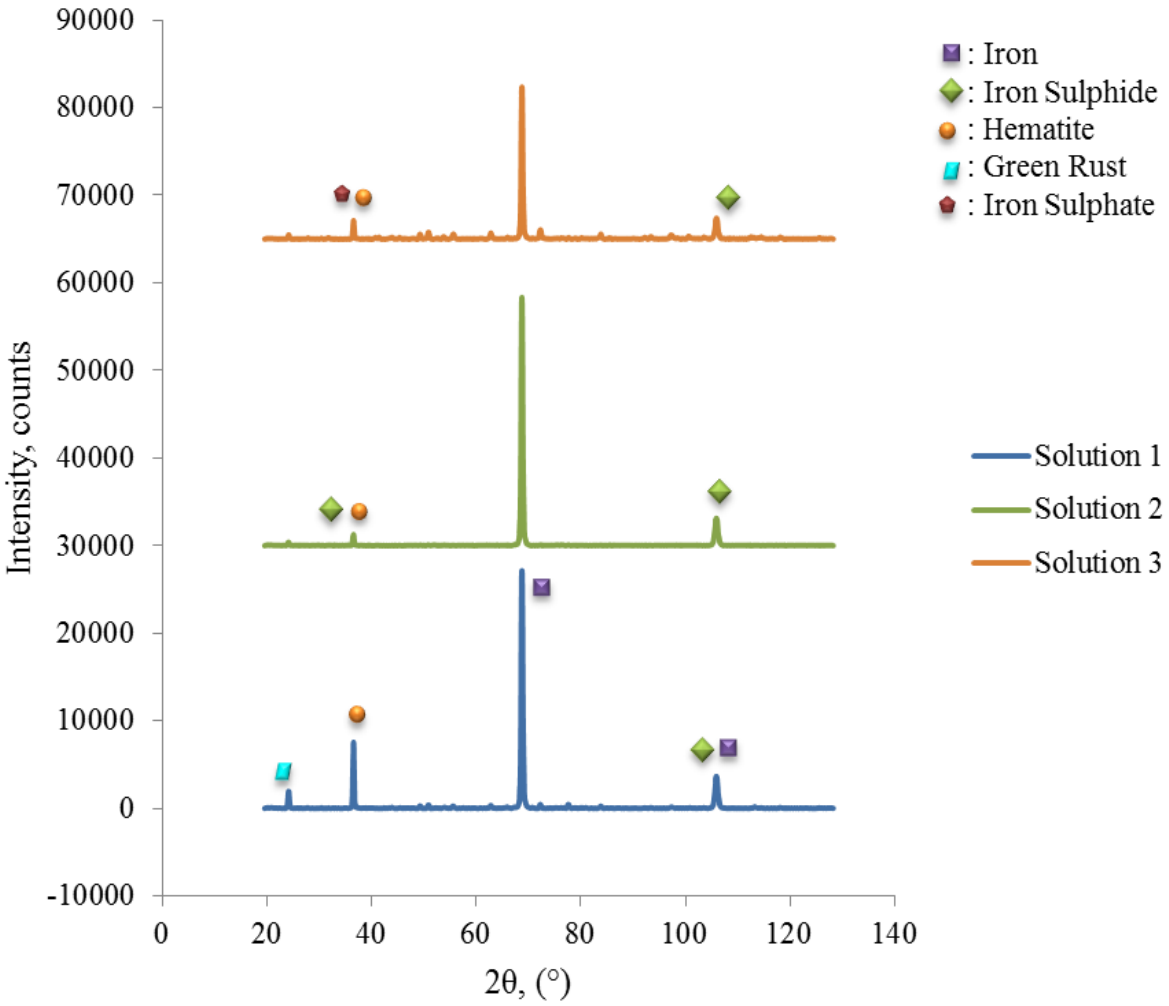

Fig. B.2. X-ray diffraction pattern of the corrosion products formed on the bottom of the crevices after immersion for 60 days at room temperature, Solution 1: 10 g l^{-1} H_2SO_4, 1 g l^{-1} NaCl, Solution 2: 10 g l^{-1} H_2SO_4, 3 g l^{-1} NaCl, Solution 3: 50 g l^{-1} H_2SO_4, 1 g l^{-1} NaCl